NEUTRON ACTIVATION MEASUREMENTS FOR MATERIALS USED IN FUSION REACTORS

Yit-Fong Chan

Submitted for the degree of

Master of Science (by Research)

in Physics

Department of Physics

University of York

Heslington

York

YO10 5DD

September 2012

ABSTRACT

Today's high demand for power (electricity) is dominantly supplied from power stations burning fossil fuels. At the risk of depletion of the Earth's supply of fossil fuel, developments in alternative sources of power include nuclear power and renewable energy (e.g. wind turbines). Current nuclear power plants rely on fission reactors which generates significant amount of energy but at the cost of unwanted radioactive by-products. Fusion power is seen as an alternative source of electricity in the future, producing less waste than their fission counterpart. Understanding how materials behave under the influence of a high flux of neutrons will be valuable towards the future design of the fusion reactor.

Analysis from neutron activated foils resulted in cross-section measurements that were a few order of magnitudes larger than published values (Jendl 4.0). To suppress background contributions to the detector, an anticoincidence system was developed at the University of York. The system utilise both passive and active shielding, for the latter, a plastic scintillator (BC404, Saint-Gobain Crystals) was used to veto contribution from (high energy) cosmic rays that can be registered in the primary detector (Ge(Li), Ortec). Experiments using a ^{22}Na calibration source saw a reduction of counts of 45% and 36% in the 511keV and 1274keV photopeaks respectively.

A current material of interest is a PAK alloy predominantly made up of iron, where small foil samples where irradiated at the ASP facility (AWE Aldermaston, UK) to observe for reoccurring reactions and the induced activity of the foil itself. Data from three experiments (*EXPT92*, *EXPT93*, and *EXPT102*) were provided by Steven Lilley (Culham Centre for Fusion Energy). From the identified γ-ray peaks from the *EXPT92* dataset (sample), the induced activity of a 1g test sample irradiated for 5 minutes, had an equivalent dose-rate (in air) of 13.4nSv.hr^{-1} at 1m.

ACKNOWLEDGEMENTS

Firstly I would like to thank my supervisor Dr David Jenkins for his guidance and patience throughout the year on this project.

Special thanks to Steven Lilley, Lee Packer, Dr Raul Pampin, and Dr Andrew Davis (Culham Centre for Fusion Energy) for their valued advice and their kind invitation to Culham, Oxfordshire. I would also like to thank Dr Simon Fox for installing the FLUKA package onto the computer system, Dr Pankaj Joshi for his technical advice in the research laboratory and helping me when the NIM-BIN malfunctioned, Dr Paul Davies for his assistance using RadWare, and David Coulthard from research services for helping me move the Ge(Li) detector into the lead castle and his technical advice in the laboratory.

A big thank you to all the PhD students, Post-doctoral researchers, and other academic staff for welcoming me into Nuclear Physics Group and their valued friendship making my research year enjoyable. Finally I would like to thank my friends and family for their continued support over the past year.

DECLARATION

I declare that the work presented in this dissertation, except where otherwise stated, is based on my own research and has not been submitted previously for a degree in this in this or any other university.

Yit-Fong Chan.

TABLE OF CONTENTS

LIST OF FIGURES

LIST OF TABLES

1. INTRODUCTION

In 1960, HMS Hornbill (Culham airfield) near Oxford was acquired by the United Kingdom Atomic Energy Authority (UKEA) for nuclear research. Today it is known as the Culham Science Centre where Culham Centre for Fusion Energy (CCFE), the UK's national laboratory for fusion research, is the home of the famous Joint European Torus (JET) and Mega Amp Spherical Tokamak (MAST) experiments[1].

There is a heavy demand for energy (power) at a global scale. A large proportion is sourced from burning fossil fuels such as coal but at the cost of carbon dioxide emissions and depletion of the Earth's supply. An alternative source is nuclear power which in 2011 contributed 17.8% of the UK's annual electrical power production[2]. The understanding of nuclear physics, more specifically nuclear fission, led to the development of nuclear power via fission reactors. For simplicity, fission is the break-up of heavy nuclei into 2 equal fragments (and fission fragments) releasing energy of the order of 200MeV per fission. The kinetic energy is harnessed to produce electrical power, via a steam turbine generator similar to coal power stations, at a commercial level. Although significant amount of power is produced, unfortunately the chain-reaction leads to various unwanted (long-lived) fission products and actinides referred to as radioactive waste. An alternative is nuclear fusion which is the process of fusing light nuclei at very high temperatures releasing energy, a process is commonly seen in the Sun and other stars.

The ultimate goal at CCFE is to utilise fusion power at a commercial level by fusing deuterium $\left({}^{2}H\right)$ and tritium $\left({}^{3}H\right)$, at very high temperatures above 100 million degrees Celsius. This can be achieved by containing the reaction inside a tokamak. At high temperatures the nuclei become a plasma state and fuse producing α-particles $\left({}^{4}He\right)$ and 14.1MeV neutrons as illustrated in fig. (1.1). The energy from the neutrons is absorbed to drive a conventional steam turbine generator. The advantages of fusion include: the high abundance of ${}^{2}H$ and ${}^{3}H$ (strictly ${}^{3}H$ is naturally quite scarce however escaping neutrons from the plasma may interact with the lithium blanket within the vessel producing ${}^{3}H$ – a process known as tritium breeding), no carbon dioxide emissions, and no long-lived radioactive waste products[1,3].

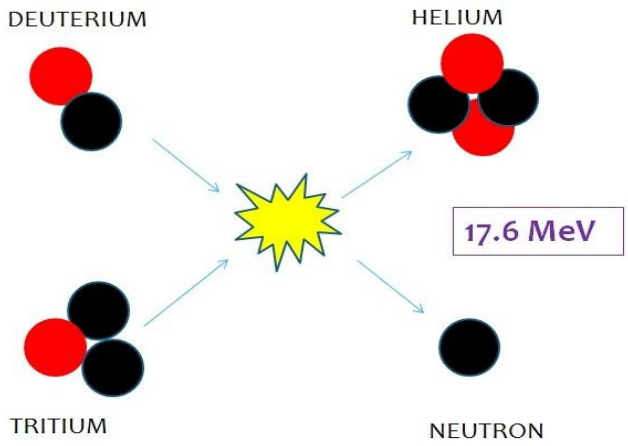

FIGURE [1.1]: (D,T) reaction resulting in 3.5MeV α-particles and 14.1MeV neutrons.

Currently the CCFE are heavily involved in the International Thermonuclear Experimental Reactor (ITER) project. ITER will be roughly 2-3 times the size of JET, proposing to produce 500MW of power from 50MW input. Construction began in 2010 on the ITER site located in Cadarache, France, aiming for completion by 2019 and starting the deuterium-tritium operation in 2027. Research and development with ITER will lead to the development of the Demonstration Power Plant (DEMO)[3]. Fig. (1.2) below shows an image of JET (UK) and ITER (France).

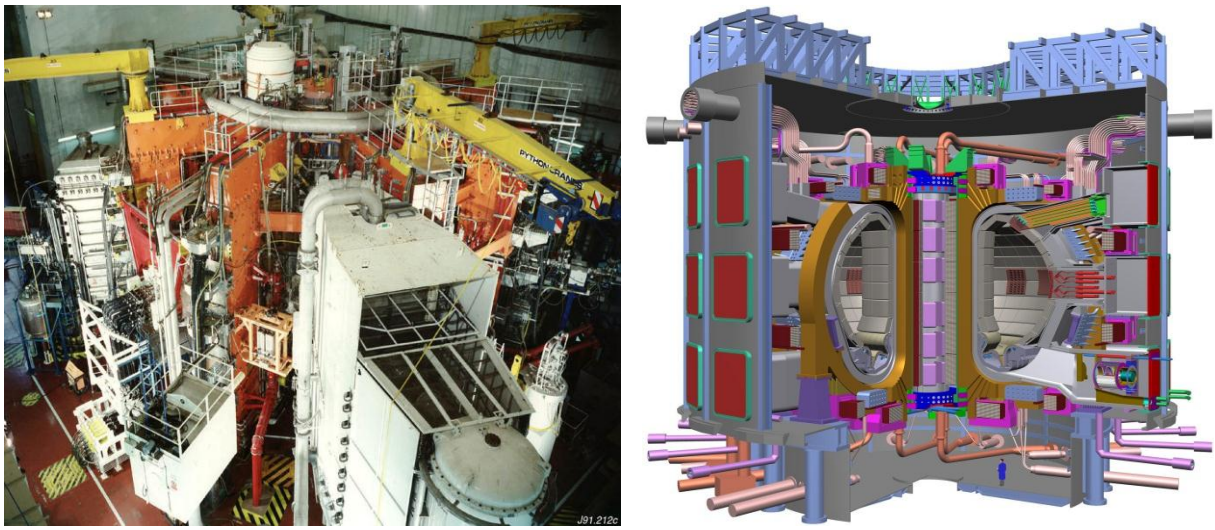

FIGURE [1.2]: JET (left) and proposed design for ITER (right). Images taken from www.ccfe.ac.uk and www.iter.org respectively.

Due to the nature of the reaction it is important to understand how materials behave under a high flux of energetic neutrons. Research on neutron activated materials will be beneficial in the future of reactor design and technology. The MSc. project focuses on the nuclear technique known as Neutron Activation Analysis (NAA) where a stable target is bombarded by neutrons inducing neutron capture. At the nuclear level, the nuclide can be in an excited state due to an excess of neutrons. The radionuclide will decay emitting characteristic γ-rays which can be detected using a high resolution detector, typically a high purity germanium (HPGe) detector. The NAA technique, which is also employed in forensics and homeland

security, is known for yielding significant results just from irradiating a small sample typically weighing less than 1g.

To be familiar with the analysis technique, data from neutron activated target foils were provided by Steven Lilley (CCFE). The measured neutron cross-sections were found to be larger than the values published on Jendl-4.0 database. The cross-section measurements are related to the number of counts detected so one approach is to minimise background contribution which is achieved using passive shielding (lead castle) and active shielding using a secondary detector. The active shielding component was developed at the University of York where a plastic scintillator was setup to veto background radiation (cosmic rays) impinging on the Ge(Li) detector via coincidence counting. A material of interest at the CCFE in an alloy called PAK450. The data from the neutron activated alloy (also provided by Steven Lilley) was analysed to observe common reactions and induced activity, leading to the concept of exposure and dose rate (radiation protection) of the activated alloy.

Monte-Carlo simulations were performed using a program called FLUKA (via Flair interface). An input file was created to replicate the HPGe detector and the experimental setup at the CCFE. By simulating pulse height spectra of a given source, it is possible to compare the expected and experimental detector efficiency of the HPGe detector.

2. THEORETICAL CONSIDERATIONS

2.1 NUCLEAR PHYSICS CONCEPTS

$$ {}^{A}_{Z}X_{N} $$

FIGURE [2.1]: Notation for element *X* with *Z* protons and *N* neutrons. The atomic weight *A* is the sum of *Z* and *N*.

An atomic nucleus made up of protons (*Z*) and neutrons (*N*) is the central component of an atom. Fig. (2.1) is a common notation which describes a specific nucleus. Isotopes refer to nuclides which have the same *Z* but different atomic mass (*A*) due to variation in *N*, an isotone is a nuclide with the same *N* but different *Z*, and nuclides with the same *A* are known as isobars[4].

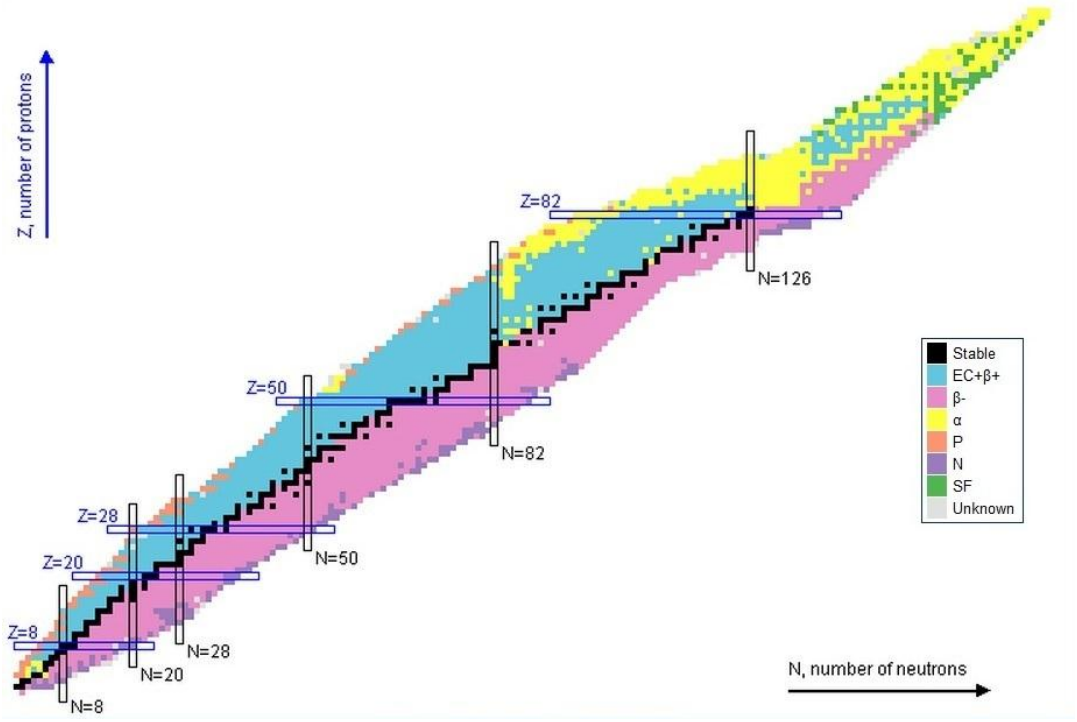

FIGURE [2.2]: The Segré chart. The colour scheme illustrates the various decay modes, where the stable nuclides are marked in black (line of stability). Image taken from National Nuclear Data Centre (http://www.nndc.bnl.gov/chart).

The occurrence of nuclei reveals informative detail regarding nuclear structure. The table of nuclides (previously known as the Segré chart, fig. (2.2)) presents stable and unstable nuclei with respect to their proton and neutron number. An unstable nuclide becomes stable by ejecting a portion of itself or emitting γ-rays. In reference to the Segré chart unstable nuclei will decay towards the line of stability with the following processes; α-decay, β-decay, and γ-

emission[4,5,6]. The figure below illustrates the possible decay pathways for a given unstable radioisotope.

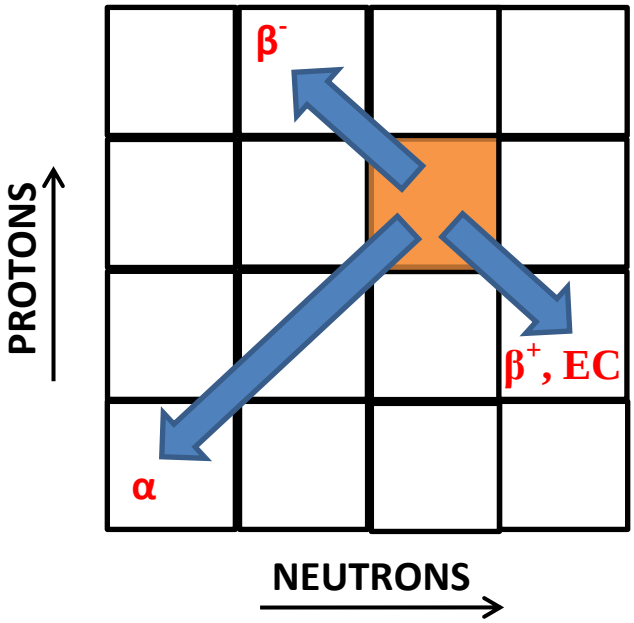

FIGURE [2.3]: Change in atomic mass from common radioactive decay modes.

The radioactive decay law states that the number of radioactive atoms at time *t*, $N(t)$, is governed by the expression,

$$N(t) = N_0 e^{-\lambda t} \tag{2.1}$$

Where N_0 is the initial number of atoms and λ is the decay constant for a given radionuclide which is related to the half-life $t_{1/2}$,

$$\lambda = \frac{\ln(2)}{t_{1/2}} \tag{2.2}$$

The activity *A* is the number of decaying atoms (or disintegrations) per unit time,

$$A = \frac{dN}{dt} = -\lambda N \tag{2.3}$$

The unit "disintegrations per second" is commonly referred to as the Becquerel (Bq). The Curie (Ci) is an older unit for activity which is equivalent to 3.7×10^{10}Bq.

In turn the decay equation can be written as,

$$A(t) = A_0 e^{-\lambda t} \tag{2.4}$$

2.1.1 α-DECAY

Heavy unstable nuclei (Z > 80) will generally undergo α-decay. During this process an α-particle is ejected from the nucleus in the form of ^{4}He. α-particles are classed as heavy charged particles, they can be highly energetic (which is also discrete) but have a relatively low velocity due to its mass. This implies that they have low penetrating characteristics such that they lose their energy as they interact with matter. α-particles typically have a range of a few centimetre in air, decreasing further with denser materials. An expression for α-decay is,

$$ {}^{A}_{Z}X \rightarrow {}^{A-4}_{Z-2}Y + {}^{4}_{2}He + Q $$

$$ Q = (M_X - M_Y - M_\alpha)c^2 \tag{2.5} $$

Where Q is energy released, M is the mass and c is the speed of light. During this type of decay process the half-life is long typically of the order of years.

2.1.2 β-DECAY

β-decay is the emission of either electron (e^-) or positron (e^+). If the nucleus is neutron-rich a neutron can transform itself into a proton by a process known as β$^-$-decay

$$ n \rightarrow p + e^- + \bar{\nu} $$

$$ {}^{A}_{Z}X \rightarrow {}^{A}_{Z+1}Y + {}^{0}_{-1}e + \bar{\nu} + Q $$

$$ Q = (M_X - M_Y)c^2 \tag{2.6} $$

Similarly for proton-rich nucleus (β$^+$-decay),

$$ p \rightarrow n + e^+ + \nu $$

$$ {}^{A}_{Z}X \rightarrow {}^{A}_{Z-1}Y + {}^{0}_{1}e + \nu + Q $$

$$ Q = (M_X - M_Y - 2m_e)c^2 \tag{2.7} $$

Where ν and $\bar{\nu}$ are the neutrino and antineutrino respectively. An alternative decay mode for a proton-rich nucleus is electron capture, in which a proton and an electron are transferred into a neutron and a neutrino.

$$ p + e^- \rightarrow n + \nu $$

$$ {}^{A}_{Z}X + {}^{0}_{-1}e \rightarrow {}_{Z-1}{}^{A}Y + \nu + Q $$

$$ Q = (M_X - M_Y)c^2 \tag{2.8} $$

β-decay has a characteristic continuous energy spectrum where the peak is the average energy and the end-point is the maximum energy. Thin sheets of metal (e.g. aluminium sheet of a few millimetres thick) are commonly used to attenuate β-particles. The half-life can vary in the order of magnitude from a few minutes to a few weeks (months).

2.1.3 γ-EMISSION

A radionuclide in an excited state decays to another state (which may be excited or ground state) by emission of a photon in the form of γ-rays which arise from transitions within the nucleus, or X-rays arising from transitions within the atomic shell. γ-rays typically follow α and β-decays since these decay modes often lead to an excited daughter nucleus.

Emitted γ-rays have energies ranging from a few keV to an order of MeV, with relatively short half-lives typically measure in seconds (in some cases in hours). Photons are the most penetrative of the 3 modes of decay, where lead blocks are commonly used to attenuate γ-rays.

2.2 INTERACTIONS OF PHOTONS WITH MATTER

Photons (X-rays and γ-rays) interact through 3 mechanisms; Photoelectric Effect, Compton Scattering, and Pair Production[6,7].

2.2.1 PHOTOELECTRIC EFFECT

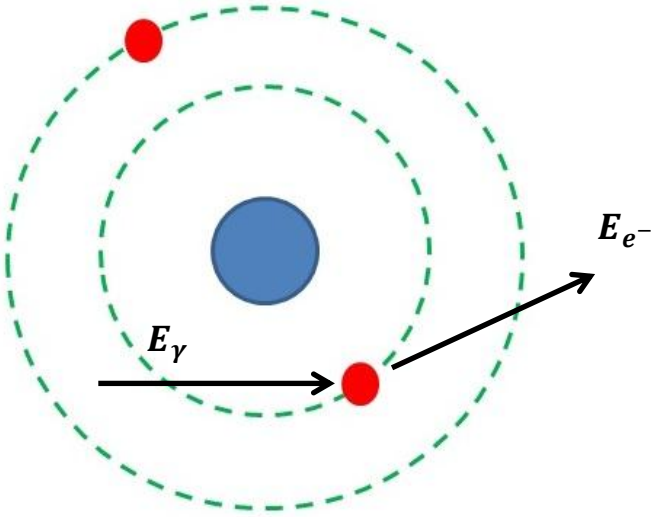

FIGURE [2.4]: Concept of photoelectric effect.

During photoelectric effect, the entire photon energy E_γ is transferred to a bound electron. The electron gains sufficient to be ejected from its orbit thus becoming a photoelectron with energy E_e-.

$$E_e\text{-} = E_\gamma - E_b \tag{2.9}$$

Where E_b is the binding energy of the electron, and E_γ is the product of Plank's constant h and frequency v. The ejected electron leaves a vacancy in the shell (fig. (2.4)), an electron from an outer shell may de-excite and "drop down" whilst emitting X-rays to occupy the vacancy. The de-excitation is known as Auger electrons. The cross-section (or probability) σ is proportional to the atomic number and incident photon energy,

$$\sigma_{PE} \propto \frac{Z^{4-5}}{{E_\gamma}^{3.5}} \tag{2.10}$$

From the expression it is seen that the Photoelectric effect is dominant low energy photons and high-Z materials.

2.2.2 COMPTON SCATTERING

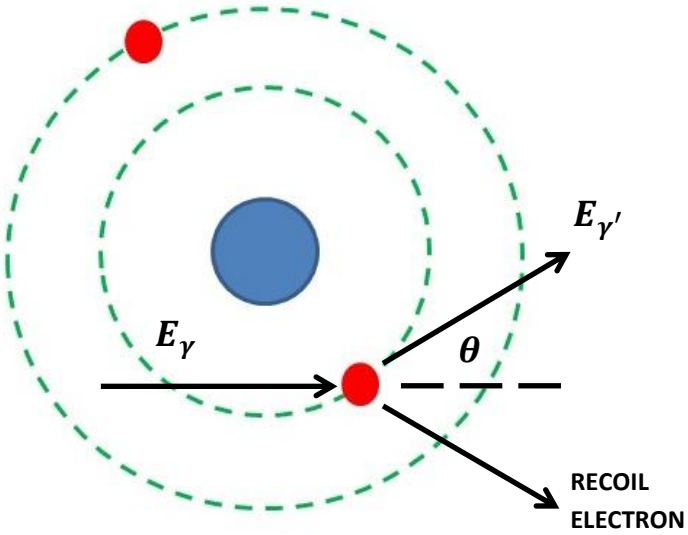

FIGURE [2.5]: Concept of Compton scattering.

Compton scattering occurs when the incident photon is deflected from its path at an angle θ, which collides with as electron at rest (see fig (2.5) above). Due to conservation of momentum, some of the photon energy is transferred to the electron, in turn the recoil electron is rejected from its shell. The scattered photon energy $E_{\gamma'}$, can be determined by the expression,

$$E_{\gamma'} = \frac{E_\gamma}{1 + \frac{E_\gamma}{m_0 c^2}(1 - \cos\theta)} \tag{2.11}$$

Where m_0 is the electron rest mass and c is the speed of light (the product m_0c^2 is commonly referred as the rest mass energy). Due to the scattering of photons at various angles the probability of interaction is governed by the Klein-Nishina formula (differential cross-section),

$$\frac{d\sigma}{d\Omega} = Zr_0^2\left(\frac{1}{1+\alpha(1-\cos\theta)}\right)^2\left(\frac{1+\cos^2\theta}{2}\right)\left(1+\frac{\alpha^2(1-\cos\theta)^2}{(1+\cos^2\theta)\left(1+\alpha(1-\cos\theta)\right)}\right) \quad (2.12)$$

Where $\alpha \equiv h\nu/m_0c^2$ and r_0 is the classical electron radius. For simplicity in terms of material (Z-number) and energy,

$$\sigma_{CS} \propto \frac{Z}{E} \quad (2.13)$$

2.2.3 PAIR PRODUCTION

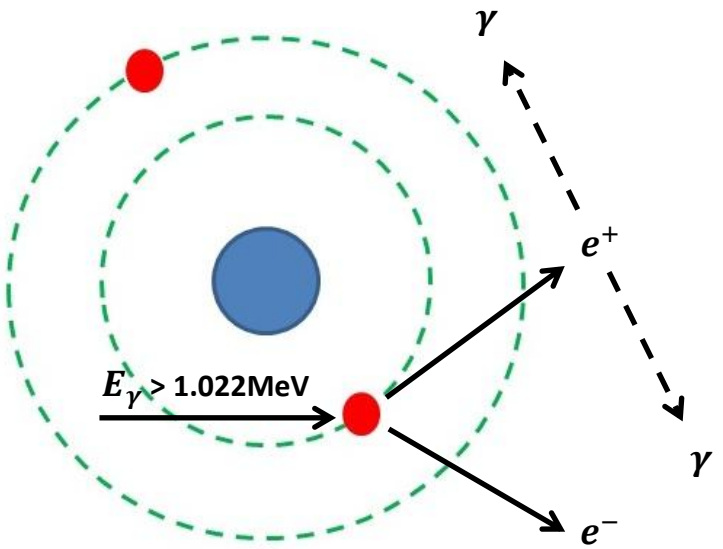

FIGURE [2.6]: Concept of pair production.

Photon energies in excess of twice the rest mass energy ($2m_oc^2$ = 1.022MeV) the photon energy can be completely converted into the production of electron-positron (e^-- e^+) pair. As shown in fig. (2.6) the positron can collide with electron and undergo an annihilation process such that 2 γ-rays (511keV each) are emitted back to back. The kinetic energy is,

$$E_K = E_\gamma - 2m_0c^2 \quad (2.14)$$

The pair production cross-section increases roughly with the kinetic energy and the material,

$$\sigma_{PP} \propto Z^2 E_\gamma - 2m_0c^2 \tag{2.15}$$

2.2.4 ATTENUATION

Consider a beam of photons passing through a medium. It is seen that the intensity of the beam after interacting with the medium (the transmission) is lower than the incident beam. This phenomena is known as attenuation. Following the Beer-Lambert law, the transmission is related to the material and length of the target.

$$I_x = I_0 e^{-\mu x} \tag{2.16}$$

Where I_0 is the incident intensity, I_x is the transmission, x is the absorber thickness, and μ is the attenuation coefficient of a given material. The linear attenuation coefficient is commonly used to describe the attenuation per unit length, whereas the mass-attenuation coefficient (quoted in units of area per unit mass) takes into account the density of the material.

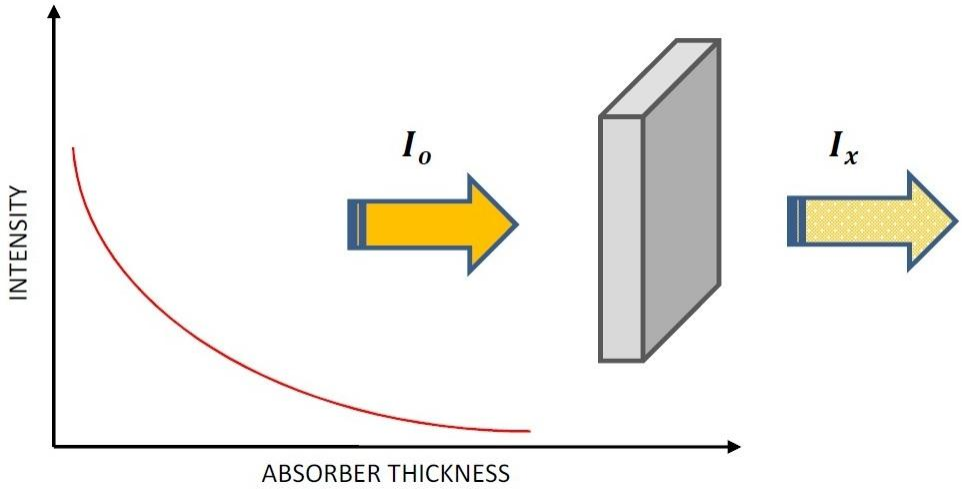

FIGURE [2.7]: Intensity diminishing with thickness.

Shown by the exponential decay in fig. (2.7), photons are not stopped indefinitely (they have infinite range) however, the intensity can be reduced dramatically using relevant shielding such as lead (high Z material). The total attenuation coefficient is the sum of the 3 interaction mechanisms,

$$\mu = \mu_{PE} + \mu_{CS} + \mu_{PP} \tag{2.17}$$

Fig. (2.8) illustrates how the interaction mechanisms contribute towards the attenuation coefficient for germanium as a function of photon energy. The figure shows 3 distinct regions corresponding to the photoelectric effect, Compton scattering, and pair production mechanisms. Significant attenuation (or absorption) occurs at relatively low energies (<100keV for the case of germanium) as a result of the photoelectric effect. As the photon energy increases, the photoelectric effect becomes less dominant and in turn the level of

attenuation decreases. Compton scattering becomes dominant at energies between ~200keV to a few MeV. As with the photoelectric effect, the attenuation coefficient decreases further with energy however the rate of change (with respect to energy) is not at severe. Pair production is dominant at higher energies beyond a few MeV where the attenuation coefficient slowly increases with energy and, in the case of germanium, plateaus to a constant value. The step (sudden increase in attenuation coefficient) on far left of the graph is known as the K-edge which corresponds to the energy required to eject a K-shell electron (innermost shell of the atom)[5]. Minimum attenuation occurs at energies where Compton scattering and pair production mechanisms are equal (about 7MeV seen in germanium).

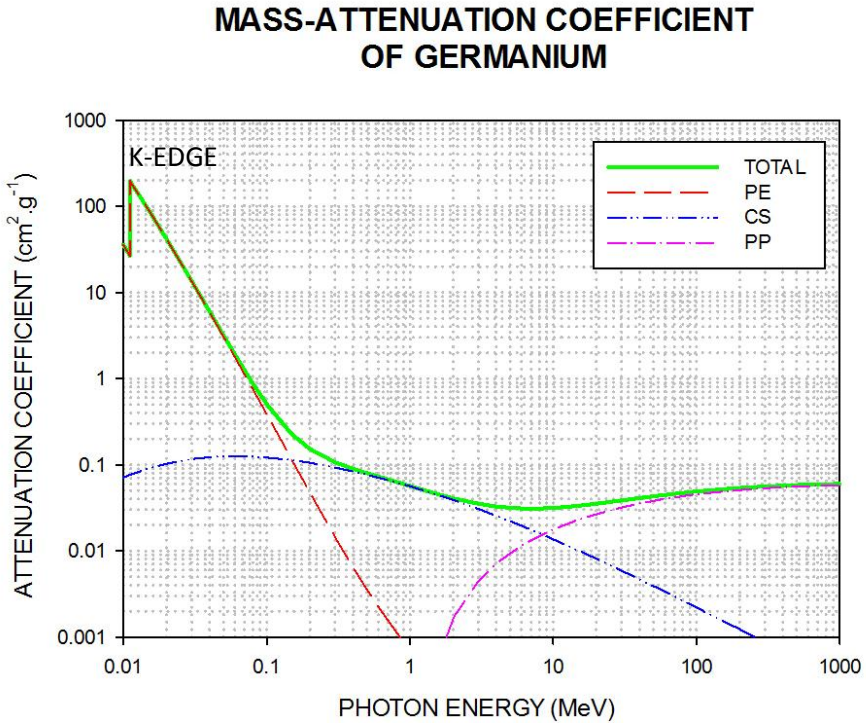

FIGURE [2.8]: Mass-attenuation coefficient as a function of energy for germanium. The figure illustrates the individual contributions due to the photoelectric effect (PE), Compton scattering (CS), and pair production (PP). The K-edge occurs at 11keV. Data taken from XCOM: Photon Cross Sections Database (National Institute of Standards and Technology, http://www.nist.gov/pml/data/xcom/index.cfm).

The interaction mechanisms vary according to the absorber material and γ-ray energy as shown in fig. (2.9). An ideal characteristic of a radiation detector, in terms of γ-spectroscopy, is to maximise energy absorption via the photoelectric effect. Fig. (2.9) shows that high Z materials are good candidates for radiation detectors[6].

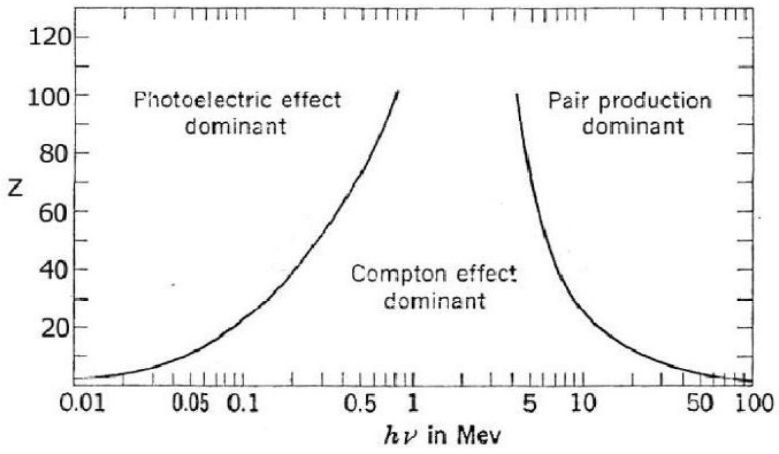

FIGURE [2.9]: Dominance of the interaction mechanisms at various energies for a given Z-material. Image taken from *Radiation Detection and Measurement*, G. Knoll. p52.

2.3 RADIATION DETECTORS

The knowledge on how radiation interacts with matter can be exploited to manufacture detectors for a given type of radiation. Radiation detectors are commonly categorised into 3 types; gas, scintillator, and semiconductor[6]. Table (2.1) is a summary of these classifications.

DETECTOR TYPE	REMARKS
GAS	Simplest type of detector which measures ionisation produced (ion-electron pairs) in the gas. The Geiger-Müller (GM) tube is a common gas detector which measures the intensity of a given source unfortunately there is no information on energy deposition.
SCINTILLATOR	Scintillators measure the light induced within the scintillator crystal from a radiation event, which is converted into a current pulse and amplified via a photomultiplier tube (PMT). Scintillators such as NaI have good efficiency with moderate energy resolution.
SEMICONDUCTOR	Semiconductors operate by measuring the charge induced from a radiation event. Depending on the material, the detector will vary among moderate efficiency and good resolution. Common examples are Si and Ge.

TABLE [2.1]: Brief description of various types of detectors.

2.3.1 HIGH PURITY GERMANIUM (HPGe) DETECTOR.

Germanium (Ge) is a well-known semiconductor material (Z=32) for γ-ray detectors and is famous for their superior energy resolution. Unfortunately they are prone to thermally induced leakage current so they require cooling with liquid nitrogen (LN_2). They were initially produced in the 1960's applied with lithium ion drifting to the Ge-crystal forming Ge(Li) detectors. By the mid-1970's high purity germanium (HPGe) detectors were commercially available. As the name suggests HPGe implies that there are less impurities in the crystal and are slightly easier to maintain. Unlike Ge(Li) detectors which need to be cooled indefinitely, HPGe detectors can settle near room temperature when not in operation. Because of the dewar, Ge-detectors are considered to be bulky however today there are smaller dewars available yielding a few hours of operating time making it portable to some extent[8]. Research in alternative cooling methods has led to the development of mains operated mechanical coolers (e.g. ORTEC X-Cooler II, www.ortec-online.com/download/X-COOLER-II.pdf) removing the need for LN_2. Eliminating the dewar will make the detector system less bulky as a whole and convenient for long/multiple experiments (no need to refill the dewar). Also, introduction of battery packs will allow mechanical coolers to be portable.

HPGe-detectors are fabricated using the Czochralski technique[8]. A seed crystal is placed inside a pool of molten germanium which is slowly withdrawn. The growth of the crystal is controlled by adjusting the temperature of the melt and the rate of withdrawl. The Hall effects are measured to determine if it is *n* or *p*-type, it is then cut into a cylinder with the face bulletised to maximise charge collection (if the end is not bulletised then the electric field lines are not radial such that there will be low field regions at the "extreme corners")

The Ge-crystal is a cylindrical can with the core removed. This is known as a coaxial configuration subdivided further into *p*-type or *n*-type depending on the contact, which ultimately governs the direction of electrons and holes drifting within the crystal[6]. Fig (2.10) illustrates the difference between the *p*-type and *n*-type detectors. As a radiation event (photon) interacts with the crystal it produces electron-hole pairs (ehp's) where the migration induces a charge proportional to the photon energy and is recorded through the acquisition system using various nuclear instrument modules (NIM's).

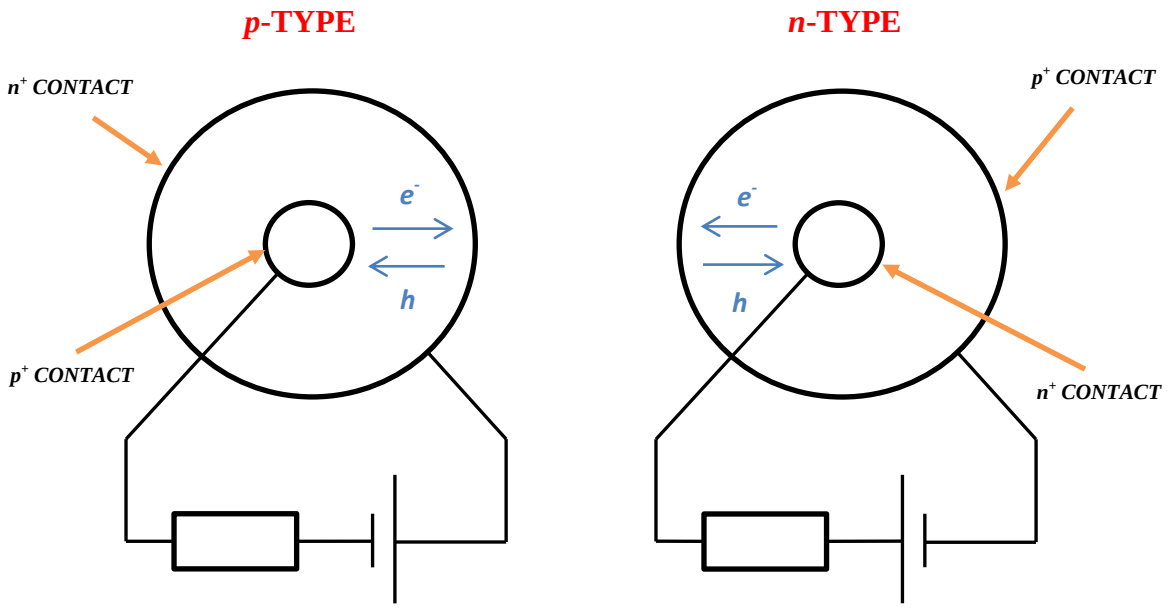

FIGURE [2.10]: Schematic of coaxial configuration. Image modified from *Radiation Detection and Measurement*, G. Knoll. p409.

2.3.2 PLASTIC BC404 SCINTILLATOR

Manufactured by Saint-Gobain Crystals, the plastic (organic) scintillator is made up of Polyvinyl-Toluene (PVT) monomer blended with a primary scintillator dye and secondary wavelength shifting dye. The pre-polymerised mixture is poured into glass moulds and placed inside an oven to allow the mixture to fully polymerise for about a week. Once cooled, the glass moulds are removed and the plastic slab is ready to be cut as required[9].

Scintillators operate differently to semiconductors that being the emission of light (fluorescence) from ionising radiation. A photomultiplier tube (PMT) is coupled to the scintillator so that the light is converted into electrical pulses and analysed using relevant NIM's. The following are properties for an ideal scintillator[6]:

- Conversion of kinetic energy of charged particles into detectable light with high efficiency.
- The light yield should be proportional to the energy deposited.
- For good light collection the scintillator should be transparent to its own emission wavelength.
- In order to generate fast pulses, the decay time of the induced light should be short.
- The scintillator material should be suitable to be manufactured in large volumes (or as required for the detector).
- The refractive index of the material should be similar to that of glass to maximise optical coupling with the PMT or equivalent light sensor.

Organic scintillators are well known for their fast pulses, are relatively cheap and can be produced in large volumes at cost of energy resolution. They are commonly used in timing experiments.

2.3.3 γ-RAY SPECTROSCOPY

In many cases, the main purpose of radiation detectors is to measure the energy distribution (spectrum) of the incident radiation[6]. This can be achieve by analysis of the pulse height distribution produced by the detector and associated equipment such as amplifies and a multichannel Analyser (MCA). The MCA collects the data (broad range of voltage pulses) and is converted into digital format via an Analogue-to-Digital Converter (ADC). The data is binned into individual channel numbers (counts per channel) producing an image known as a spectrum. For a monoenergetic source, a single peak will be observed where the spread over a range of channels reflects the fluctuations in the pulse heights produced by the detector. If the energy of the characteristic peak is known then the channel number can be translated in terms of energy (a process known as energy calibration). Strictly the random nature of radiation is described by the Poison distribution however, if good counting statistics are met then the randomness tends towards a Gaussian distribution.

The width, or the full width at half maximum (FWHM), of the energy peak describes the resolution *R*, of the detector. The FWHM is related by,

$$R = \frac{FWHM}{x_0}$$

$$= \frac{2\sqrt{2ln2}\sigma}{x_0} \tag{2.18}$$

Where x_0 is the peak centroid and σ is the standard deviation. Resolution is often quoted as a percentage or even expressed as the FWHM alone (in some cases the full width at one tenth maximum may be used).

Another property of the detector is the efficiency at which photons are detected[6,10]. The absolute efficiency (ε_{ABS}) is the ratio of events detected with respect to the events emitted of a given source. Mathematically it is defined as,

$$\varepsilon_{ABS} = \frac{C_T}{N_\gamma} \tag{2.19}$$

$$N_\gamma = AI_\gamma \tag{2.20}$$

Where C_T is the total number of counts, N_γ is the number of γ-rays emitted by the source which itself is a function of the activity *A* and the fractional intensity (branching ratio) I_γ for a given energy. The intrinsic efficiency (ε_{INT}) is the ratio of events recorded with respect to the events impinging on the detector, taking into account the solid angle Ω.

$$\varepsilon_{INT} = \frac{C_T}{N_\gamma{}'} \tag{2.21}$$

$$N_\gamma{}' = \frac{\Omega}{4\pi} N_\gamma \tag{2.22}$$

$$\Omega = 2\pi\left(1 - \frac{d}{\sqrt{d^2 + r^2}}\right) \tag{2.23}$$

Where *d* is the source detector distance and *r* is the radius of the detector can. The intrinsic photopeak efficiency (ε_{IP}) considers the energy peak so therefore it takes into account the counts under the peak C_p.

$$\varepsilon_{IP} = \frac{C_p}{N_\gamma{}'} \tag{2.24}$$

Commonly seen with Germanium detectors, the full energy peak efficiency is measured over a wide range of energies and fitted to the logarithmic function,

$$\ln \varepsilon = \sum_{i=1}^{N} a_i \left(\ln \frac{E}{E_0}\right)^{i-1} \tag{2.25}$$

Where a_i are fitted parameters and E_0 is the fixed reference energy[6].

2.4 NEUTRON ACTIVATION ANALYSIS

Neutron activation analysis (NAA) is a technique with involves a sample irradiated by neutrons to induce radioactivity[5,6,11]. Consider a target bombarded by neutrons such that neutron capture occurs. The target will either remain stable or become unstable; in the latter case the nuclei will be in an excited state and undergo β-decay emitting γ-rays which can be detected using an HPGe detector. The net rate of the radioactive nuclei is governed by the expression,

$$\frac{dN_Y}{dt} = P(t) - \lambda_Y N_Y \tag{2.26}$$

Where N_Y is the number of isotopes produced during irradiation. The rate of production *P(t)* is a function of the number of target atoms N_X, cross section σ, and neutron flux $\phi(t)$,

$$P(t) = N_X \sigma \phi(t) \tag{2.27}$$

If the flux is constant then the general solution for N_Y is,

$$N_Y = \frac{P}{\lambda_Y}(1 - e^{-\lambda_Y t}) \tag{2.28}$$

Considering an irradiation time t_0 then,

$$N_Y(t_0) = \frac{N_X \sigma \phi}{\lambda_Y}(1 - e^{-\lambda_Y t_0}) \tag{2.29}$$

The number of atoms at time *t* after irradiation can be expressed as,

$$N_Y(t) = N_Y(t_0) e^{-\lambda_Y (t - t_0)} \tag{2.30}$$

The irradiated sample may not be placed in front of the HPGe-detector immediately so counting interval from t_1 to t_2 needs to be taking into account, where t_1 denotes the waiting time and t_2 is the counting/acquisition time. Fig. (2.11) shows the behaviour of a neutron activated sample. During irradiation there is a build-up in activity. Over a long period of time the induced activity will slowly reach equilibrium (saturation) such that the rate of production and rate of destruction (decay) are equal. After irradiation the sample solely decays. The number of counts detected N_C between t_1 and t_2 is expressed as,

$$N_C(t_1, t_2) = \int_{t_1}^{t_2} \lambda_Y N_Y(t) dt \tag{2.31}$$

$$= \lambda_Y N_Y(t_0) \int_{t_1}^{t_2} e^{-\lambda_Y (t - t_0)} dt$$

$$= \frac{N_X \sigma \phi}{\lambda_Y}(1 - e^{-\lambda_Y t_0}) e^{\lambda_Y t_0} (e^{-\lambda_Y t_1} - e^{-\lambda_Y t_2}) \tag{2.32}$$

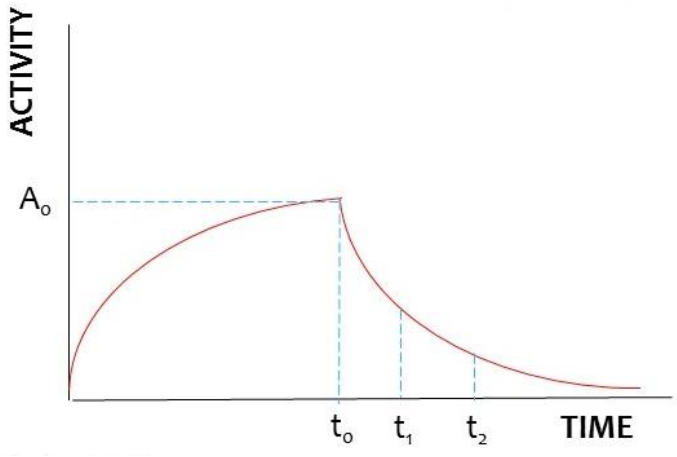

FIGURE [2.11]: Activity build-up as sample is irradiated to t_0. Counting measurements taken between t_1 and t_2.

The number of target atoms N_X (for a given isotope) is related to its natural abundance *A(%)* the atomic weight W_A , Avogadro's number N_A , and the mass of the sample *m*.

$$N_X = A(\%)\frac{mN_A}{W_A} \tag{2.33}$$

The detector response takes into account the absolute full energy peak efficiency ε_γ and the fractional intensity I_γ of the γ-ray from the particular nuclei.

$$\therefore N_C(t_1, t_2) = \frac{N_X \sigma \phi}{\lambda_Y}(1 - e^{-\lambda_Y t_0})e^{\lambda_Y t_0}(e^{-\lambda_Y t_1} - e^{-\lambda_Y t_2})\varepsilon_\gamma I_\gamma \tag{2.34}$$

2.5 BACKGROUND RADIATION

The term background radiation refers to ionising radiation which occurs naturally in the environment. Terrestrial radiation originate from the Earth's surface (rocks and soil) and are present in many building materials commonly from ^{238}U and ^{232}Th decay series as well as ^{40}K. The level of radiation varies over the Earth's surface. Cosmic rays arise in 2 forms; primary cosmic-rays are extremely energetic (GeV and greater) heavy charged particles and ions in space. They interact with the Earth's uppermost atmosphere producing a large assortment of energetic (up to order of MeV) showers of electrons, neutrons, protons, as well as pions, muons, and photons. Artificial radiations are man-made occurring from medical procedures (diagnostic and therapeutic radiology), nuclear industry, and fall out from nuclear testing, warfare, and accidents (Chernobyl and Fukushima nuclear disasters)[5,6].

Background radiation can contribute towards the detector system which varies with the type and size of the detector. Background contribution can be "controlled" using relevant shielding[6]. The more common and simplistic approach is passive shielding using dense material. Lead is the most widely used shielding because of its high atomic number (Z=82)

and density, in turn the photoelectric effect dominates at energies up to ~500keV. Only a thickness of a few centimetres can attenuate significant amounts of γ-rays. Lead is typically manufactured into interlocking blocks which gives the freedom of constructing a shield (lead castle) to a desired size. Lead is also naturally radioactive so specially refined lead (at a financial cost) is used for low-background applications. Other materials used for shielding purposes include steel (commonly used when lead alone is too expensive) and concrete (construction of large volume shielding at a low cost). It is possible to construct a specially designed laboratory (e.g. concrete walls, lead-lined plywood) and even locate the laboratory underground to reduce background radiation, however penetrative cosmic-rays can still contribute towards the counting system.

Active shielding is a technique using a secondary detector (or an array of detectors) surrounding the primary detector. Also known as an anticoincidence shielding, the process involves the rejection of pulses occurring in both detectors in coincidence to suppress background radiation. This technique is commonly used to suppress the highly energetic cosmic-rays which are capable of penetrating through conventional shielding, and therefore can penetrate through both detectors. The primary detector is commonly a semiconductor (such as HPGe) and the secondary detector is a large scintillator[6].

Depending on the application it is possible to employ both passive and active shielding as part of the detector setup. Another approach that utilises a coincidence (or anticoincidence) counting system is detector segmentation. The detector crystal is fabricated such a way to allow multiple independent readouts of separate sub-volumes of the detector[6].

3 EXPERIMENTAL PROCEDURE

3.1 HPGe & Ge(Li) DETECTOR CHARACTERISATION

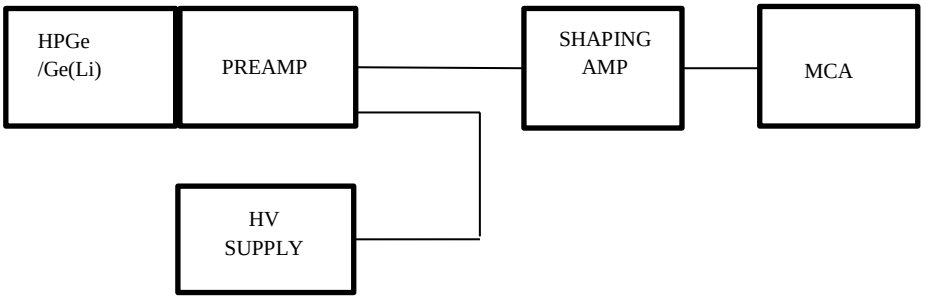

FIGURE [3.1]: Schematic of generic detector setup in the laboratory for γ-spectroscopy.

A HPGe detector was loaned to CCFE from the University of York. The detector is inside a lead castle made up of lead blocks surrounded with 1cm thick steel and a custom built lead door. The source holder is specially designed aluminium can with a Perspex base which is mounted to the detector using an adjustable stage. This yields a source-detector distance of 1.2cm.

Fig. (3.1) above is a typical setup for γ-spectroscopy. To observe the effect of shaping time on the performance of the detector, a ^{152}Eu spectrum was acquired at shaping times varying from 0.5-10μs. The detector was calibrated using ^{241}Am, ^{133}Ba, and ^{152}Eu sources (acquisition times for each source were 700s, 900s and 1200s respectively). The absolute and intrinsic efficiency of the detector can be determined from the saved spectra.

A similar experiment was setup at the University of York using a Ge(Li) detector. A ^{137}Cs calibration source was placed 3cm in front of the detector and an energy spectrum was acquired over a period of 5 minutes. Additional spectra were acquired whilst adjusting the shaping time on the amplifier.

3.2 BC404 PREPARATION AND BACKGROUND SUPPRESSION (ANTICOINCIDENCE SHIELDING)

Background suppression can be performed in 2 ways; the simplest approach is passive shielding using lead blocks. A more advance technique is active shielding by using a second detector (plastic BC404) in close proximity of the primary. As mentioned in section 2.6 the signal/output from the Ge(Li) detector will be rejected if accompanied with coincidence pulses from the BC404.

Firstly the BC404 was inspected for any physical defects in the plastic. The 2cm × 10cm × 46cm slab (sometimes referred as “the cricket bat” due to its size) coupled to a light-guide was wrapped in aluminium foil, so the induced light escapes solely through the light-guide itself, and then wrapped in black insulating tape to eliminate any external light source. The exposed surface of the light-guide was swabbed with isopropanol then a small amount of optical gel (EJ-550 Silicone Optical Grease, Eljen Technology) was carefully distributed before mounting the PMT. Thread tape (PTFE Thread Seal, Klingerflow) was used to seal the gap between the light-guide and PMT, and then finally wrapped with foil and black tape to seal and secure the PMT.

Due to the nature of background suppression, a coincidence unit is required. Fig. (3.3) illustrates the setup of the veto detector with the settings of the various modules in the NIM-BIN shown in table (3.1). An oscilloscope (LeCroy Wavejet 314 100MHz) was used to observe the response from the modules in real time.

To validate the anticoincidence setup a ^{22}Na calibration source was placed 2cm in front of the Ge(Li) detector and an energy spectrum as acquired over a duration of 30 minutes. Further spectra were acquired with passive shielding, active shielding, and a combination of both. The lead castle is lined with an inner 3mm thick copper sheet to attenuate the characteristic lead X-rays. Due to the size of the castle, 2 copper panels and a small number of lead blocks were removed to compensate for the length of the scintillator as seen in fig. (3.2).

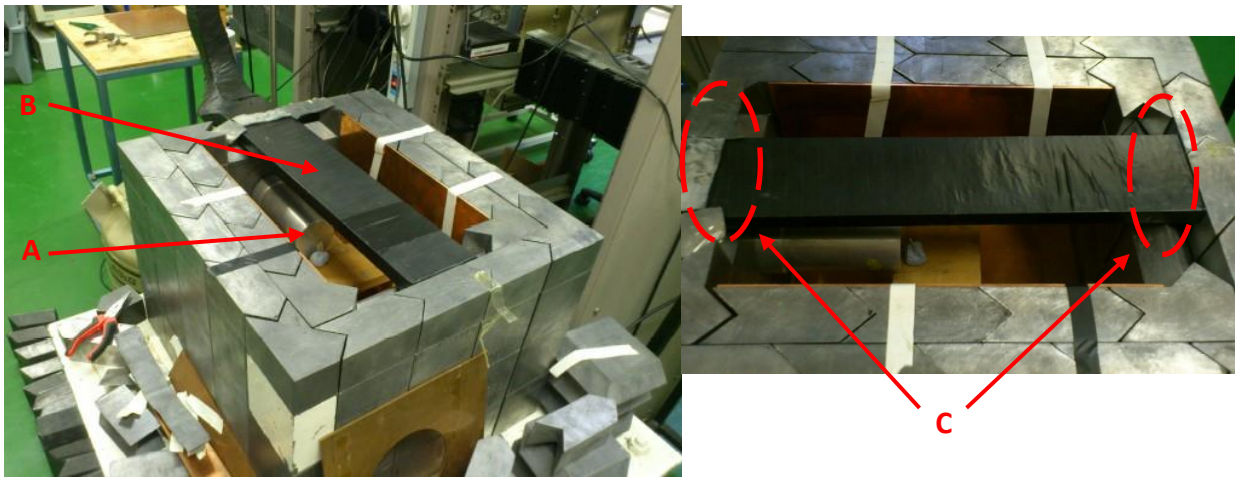

FIGURE [3.2]: Development of anticoincidence system to suppress background radiation. Ge(Li) detector (A) inside lead castle lined internally with copper sheet (to attenuate Pb X-rays) with BC404 scintillator (B) sitting above. Two copper panels and a small number of lead blocks were removed (C) to position the BC404. When in operation, a copper sheet was placed on top of the castle with another layer of lead blocks.

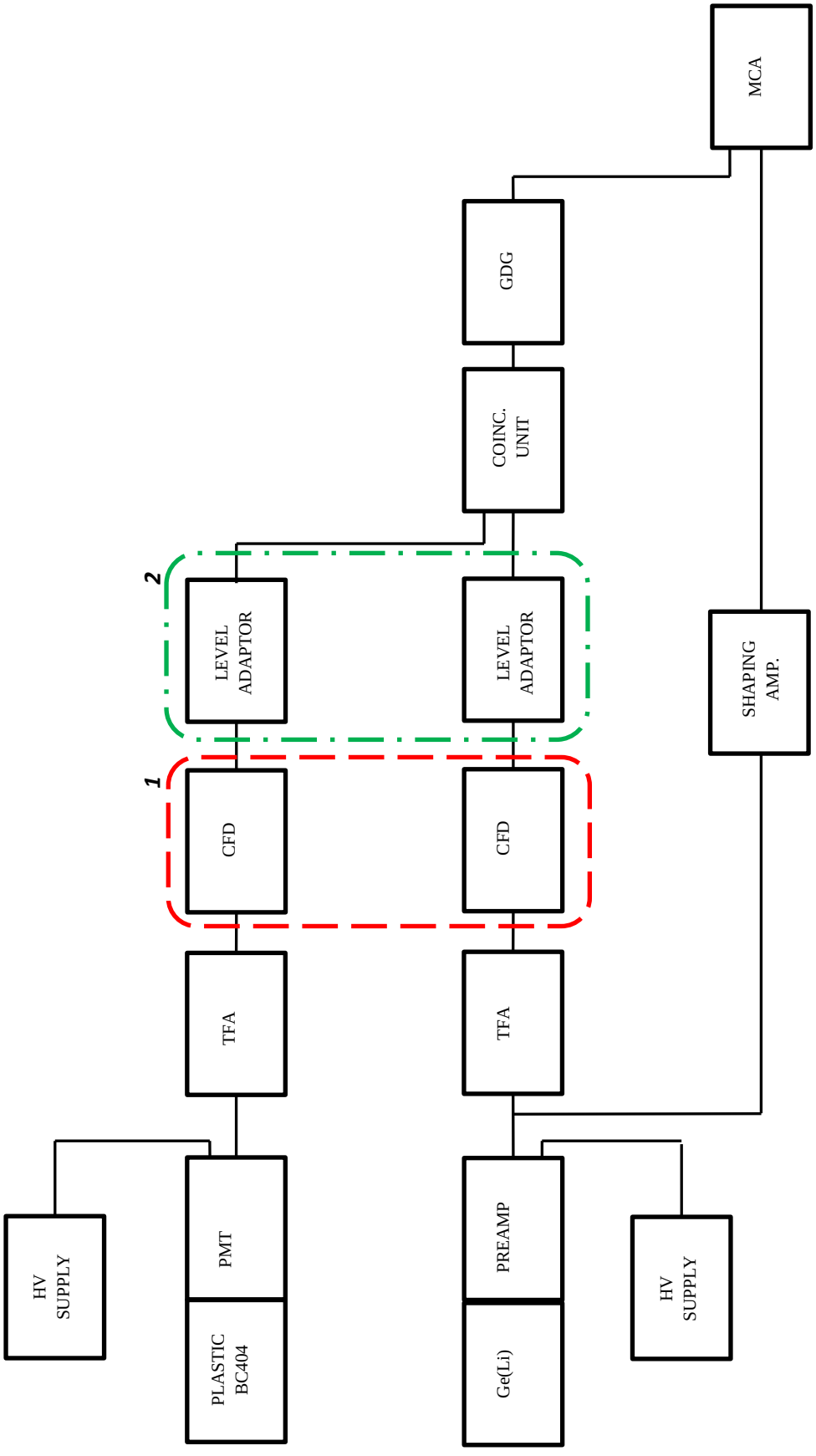

FIGURE [3.3]: Experimental setup for active shielding. [1]Lecroy 623B Octal Discriminator and [2]EG&G-ESN LA8000 Level Adaptor have multi-channel inputs. MCA is connected to PC terminal with MAESTRO software.

MODULE	SETTINGS/REMARKS	
ORTEC 556 HV POWER SUPPLY[a]	HV:	-1.7kV
ORTEC 459 HV POWER SUPPLY[b]	HV:	+3.0kV
ORTEC 474 TIMING FILTER AMPLIFIER[a]	COURSE: FINE: INT: DIFF:	×20 3 50ns OUT
ORTEC 474 TIMING FILTER AMPLIFIER[b]	COURSE: FINE: INT: DIFF:	×1 2.5 20ns OUT
LeCROY 623B OCTAL DISCRIMINATOR	CONSTANT FRACTION DISCRIMINATOR	
EG&G LA8000 LEVEL ADAPTOR	POLARITY INVERTER	
ORTEC 416A GATE AND DELAY GENERATOR	DELAY: SCALE:	7.7 1.1μs
ORTEC 418A UNIVERSAL COINCIDENCE UNIT	INPUT 1 [BC404]: INPUT 2 [Ge(Li)]:	ANTI-COINC. COINC.
ORTEC 572 SHAPING AMPLIFIER	COARSE: FINE: SHAPING:	×50 7.3 1μs

TABLE [3.1]: Modules installed in NIM-BIN. [a]Module associated with BC404. [b]Module associated with Ge(Li).

4. COMPUTATIONAL MODELLING

Monte-Carlo (MC) simulations are used to evaluate functions that are too complex to be calculated analytically commonly used in nuclear/particle transport. MC simulations rely on random number generators and require a seed (user defined starting point). Below is an example of a photon interacting with matter and the random number generated is associated to a specific interaction mechanism.

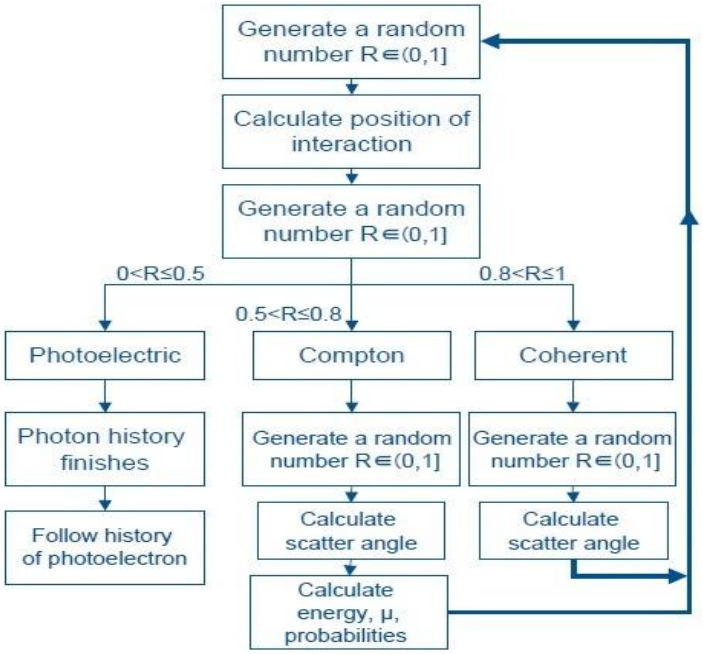

FIGURE [4.1]: Flow chart to illustrate a photon propagating through a medium. Probability of interaction: Photoelectric effect – 0.5, Compton scatter – 0.3, Coherent scatter – 0.2. Here coherent (Rayleigh) scattering is where a photon interacts with a bound orbital electron. The photon loses very little energy and scatters through at small angles. Image courtesy of Dr Silvia Pani (University of Surrey).

4.1 FLUKA

A collaboration between Italian National Institute for Nuclear Physics (INFN) and European Organisation for Nuclear Research (CERN), FLUKA[12,13] (www.fluka.org) is a particle transport code based on Fortran for applications such as detector design, dosimetry, radiotherapy, neutrino physics etc. It is capable of simulating the interaction and propagation in matter of various particles with energies ranging from 1keV to a few thousand TeV, and in special cases up to 10PeV with add-on packages.

FLAIR[14] (www.fluka.org/flair/index.html) is a common graphic user interface (GUI) for FLUKA, which operates by constructing an input file (*.inp) in the form of "cards". Each card specifies certain aspects of the system modelled or of the desired output. For example, the *BEAM* card defines the radioactive source in terms of position (Cartesian coordinates) and

energy (in GeV), *ASSIGNMA* defines the material for a given region. Fig. (4.2) is a screengrab of the FLAIR program. The cards are inserted by simply right clicking in the main window to obtain a generic list of cards (commands). The user can (to name a few) compile and debug the run-code, produce geometry plots, and process various output files within FLAIR.

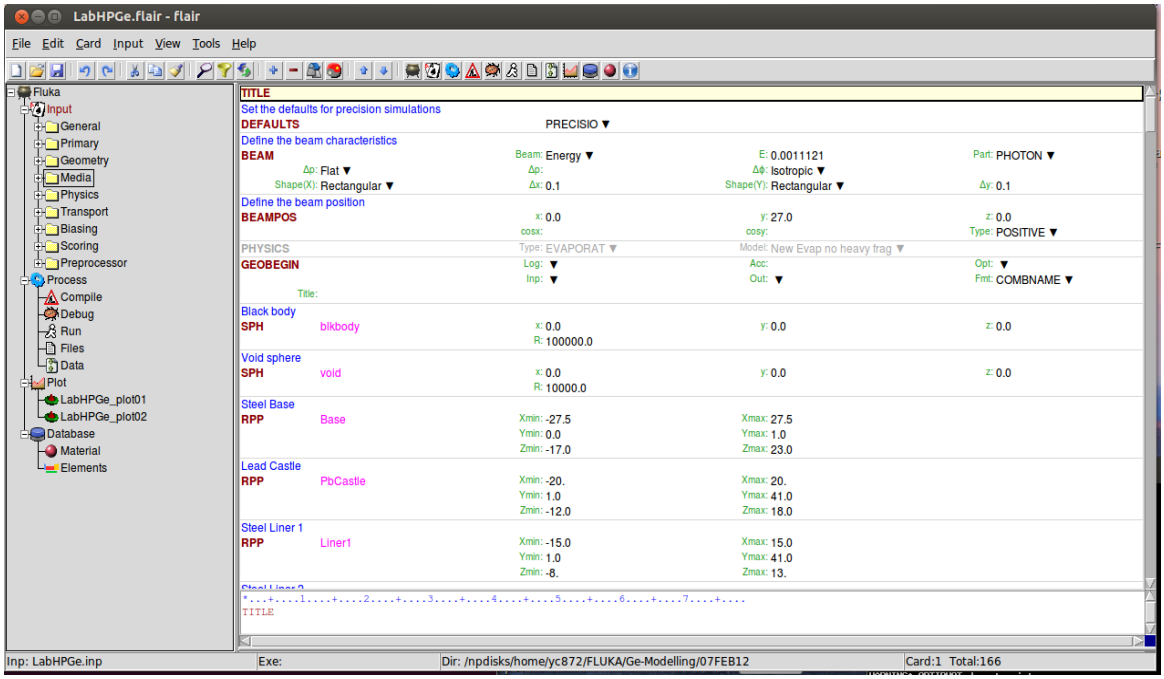

FIGURE [4.2]: Flair interface. The main window shows various user cards. The tree browser on left summaries the input file in convenient sections (e.g. Primary refers to the radioactive source/beam, and media specifies various materials to be assigned), and commands such as running the code and displaying plots.

4.2 SIMULATION OF DETECTOR RESPONSE

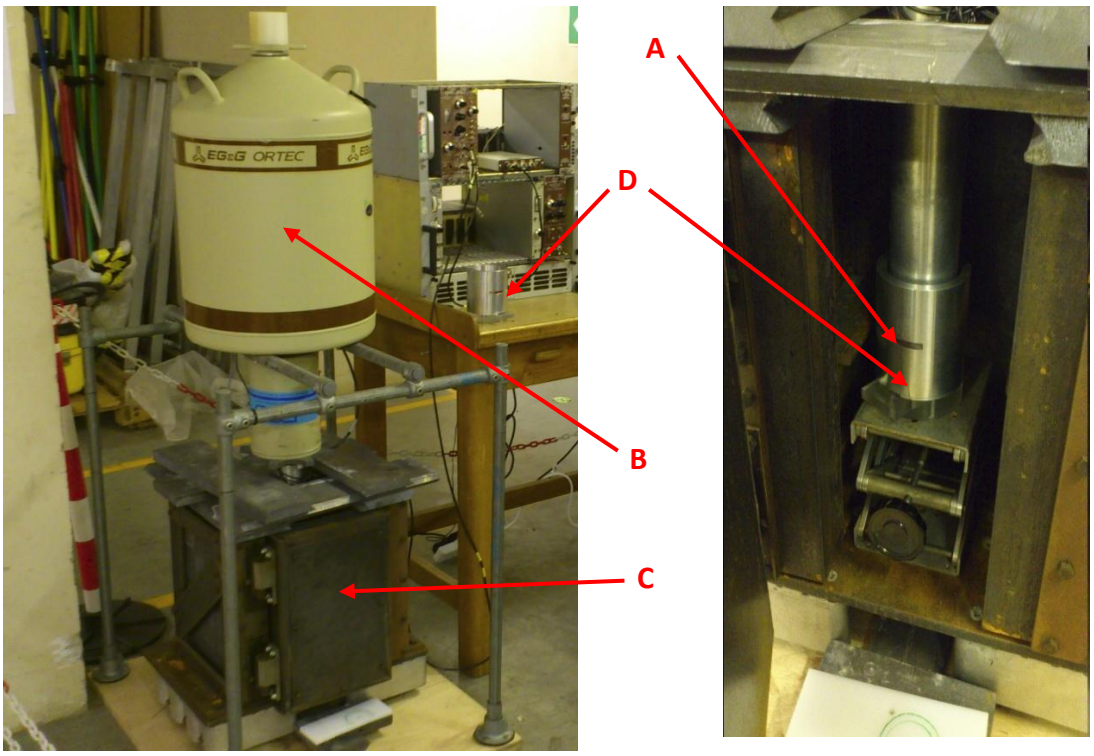

FIGURE[4.3]: Experimental setup at CCFE. HPGe detector (A) suspended on the rig with LN_2 dewar (B), pointing down inside the lead castle (C). Image on the right shows the source holder (D) coupled to the HPGe detector using a mechanical stage. Photographs taken on site with permission from Steven Lilley.

The experimental setup of the HPGe detector (manufacture specification located in appendix 1) at CCFE was replicated in FLUKA. The input file (see appendix 2) is coded such that the detector with the source holder is inside a lead castle lined with steel and custom built lead door sitting on a steel base (see fig. (4.3) above). The detector and source holder was replicated in the form of a series of cylinders (in FLUKA they are named Right Circular Cylinder, RCC) whereas the lead shielding (and hollow cavity) was based on cubes (Rectangular Parallelepiped, RPP). The germanium crystal is based on a cylindrical can (56.4mm long with 50.1mm diameter) with the face made up of various cones (Truncated Right Angled Cone, TRC) to mimic the bulletised face. In the code/input file, Ge1-4 is designated as cones and Ge5 is the remaining can. An isotropic point source was positioned in the centre of the Perspex section of the source holder about 1.2cm from the detector (the source holder is a hollow aluminium can with a Perspex base with a small compartment where the source is placed). Fig. (4.4) illustrates the geometry setup simulated in FLUKA.

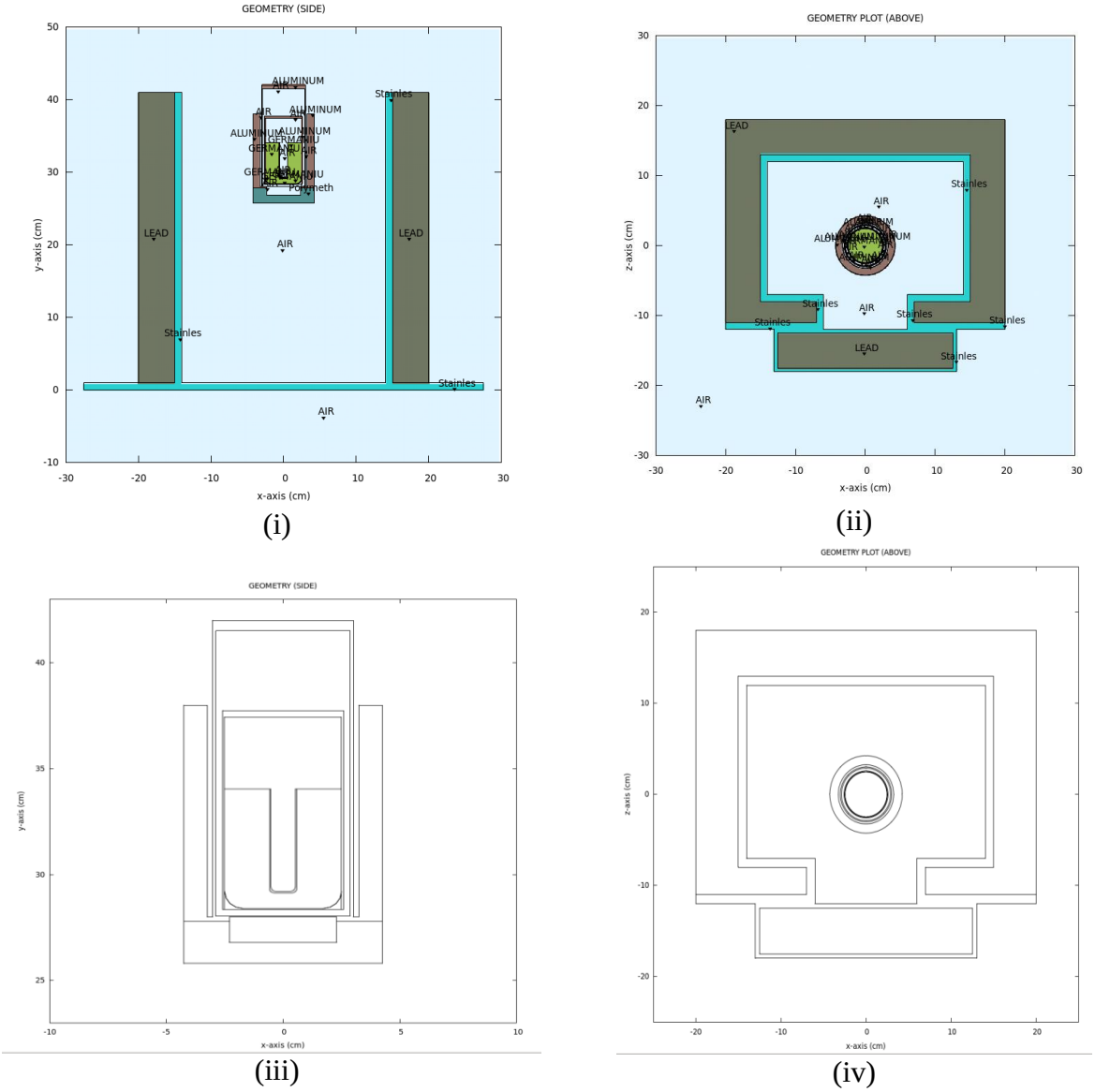

FIGURE [4.4]: Plots of the geometry setup in FLUKA. (i) side view at the centre, z = 0cm, (ii) overhead view at y = 29cm, (iii) zoomed image of Perspex source holder coupled to detector at z = 0cm, (iv) plain line drawing of overhead view (FLAIR tends to label all region when creating plots as seen in (ii)).

Porta and Campi[15] wrote a paper on HPGe detector simulations in FLUKA and showed that it is possible to produce pulse height spectra via the *DETECT* card. The function detects the number of events in a user defined region of interest (i.e. Ge1-5) within an energy range (E_{min} and E_{max}) in GeV. The number of bins/channels available is currently fixed at 1024 so for simplicity each bin is equivalent to 1keV ($E_{min} = 1 \times 10^{-9}$GeV and $E_{max} = 1.024 \times 10^{-3}$GeV). *DETECT* was implemented in the input file which in turn produced a Fortran output (*fort.17). Unfortunately reading *fort.17 was not yet implemented in FLUKA, this issue was resolved from a Fortran program *detoutput.f* located on the FLUKA online discussion forum[16]. The program was used to convert the data into an ascii file. ^{241}Am point source was simulated in FLUKA and produced a spectrum shown below.

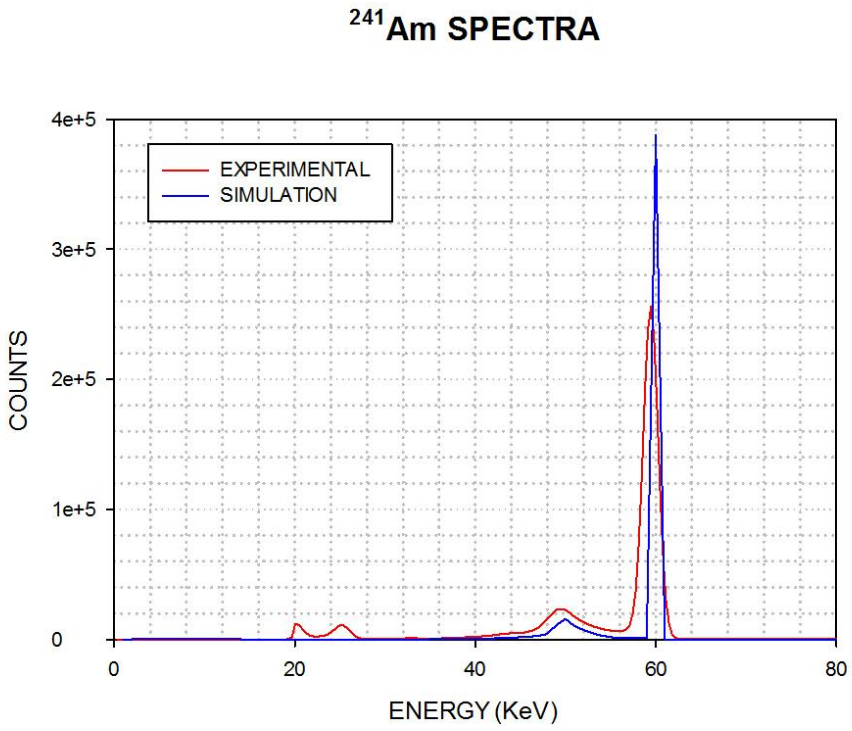

FIGURE [4.5]: Comparison of ^{241}Am, $E_\gamma = 59.5$keV ($I_\gamma = 35.9\%$). Experimental FWHM = 1.9keV. Simulation FWHM = 0.6keV.

It can be seen that the simulated energy spectrum has higher resolution in comparison to the spectrum acquired at CCFE. This is due to simulated detector system being pure; there are no impurities in the assigned materials and it does not take into account the electronics (and the associated noise) used in spectroscopy. There is also a sight offset in the lab frame of a few keV which is most likely due to the energy calibration.

^{133}Ba and ^{152}Eu calibration sources were reproduced to mimic the sources that were available at CCFE. Ideally a Fortran code that is read into FLUKA is used to simulate a non-monoenergetic source. This led to some difficulty so for simplicity each γ-emission was treated as an independent source. The initial number of photons from the source (FLUKA refers this as the number of primary histories) based on the activity of the CCFE calibration source taking into account the fractional intensity (branching ratio) and acquisition time. Below (fig. (4.6)) is the absolute efficiency of the detector. It is evident that the efficiency degrades at energies greater than 100keV as a result of Compton Scattering (Photoelectric effect becoming less dominant). The efficiency degrades further at energies greater than 1MeV because a large proportion of the incident γ-rays will penetrate through the detector with minimal interaction[6]. As before the simulation depicts an ideal response. A factor which can cause this discrepancy is the (surface) dead layer of the detector. This is the inactive region of the germanium crystal initially governed by the thickness of p+ and n+ contacts (typically < 1μm and ~100μm respectively). The surface dead layer can vary over periods of time such that the electric field and charge collection efficiency will diminish due to the formation of surface channels[6].

The active area can be determined by modifying the dimension (reducing the size) of the germanium crystal such that the simulated and experimental efficiencies are similar (although can be time consuming). It may be useful to acquire an X-ray image of the detector to observe the positioning of the crystal for future reference.

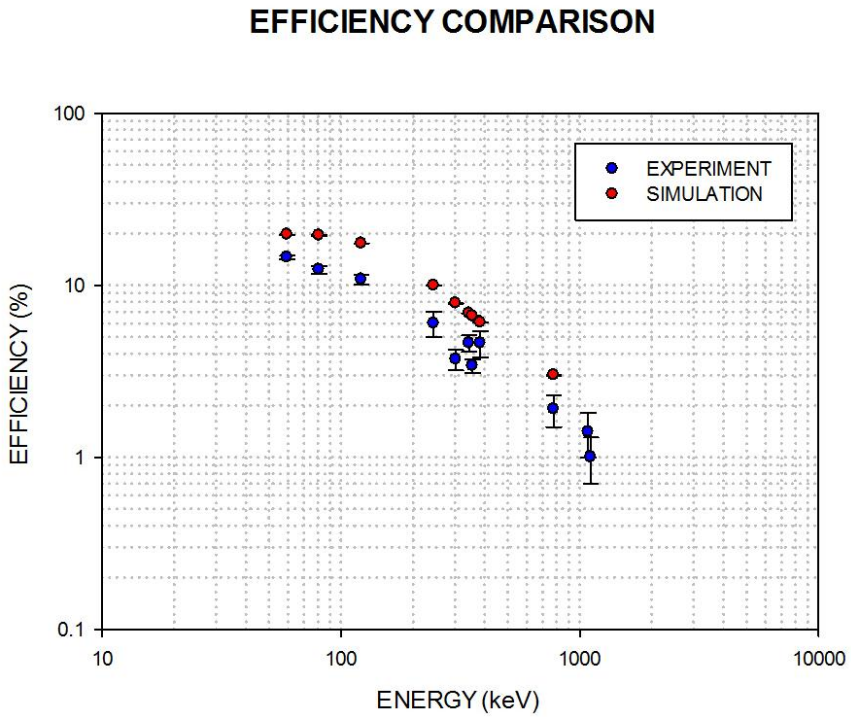

FIGURE [4.6]: Comparison of efficiency in simulation and lab-frame.

5. RESULTS AND DISCUSSION

5.1 ACTIVATION OF Mo-FOIL

The target foils were irradiated using the ASP Accelerator (AWE Aldermaston, UK) where a deuteron beam is accelerated at a tritium target inducing the (d, t) -reaction to produce 14MeV neutrons. The target foils are disc-shaped, 12mm in diameter and 125μm thick. A Pneumatic Transfer System is utilised at AWE where the foil is placed inside a capsule which positioned for irradiation for 5 minutes and then placed in front of the HPGe detector. An energy spectrum of the irradiated sample is then acquired over a duration of 15 minutes (the transport time was taken as 10 seconds)[17].

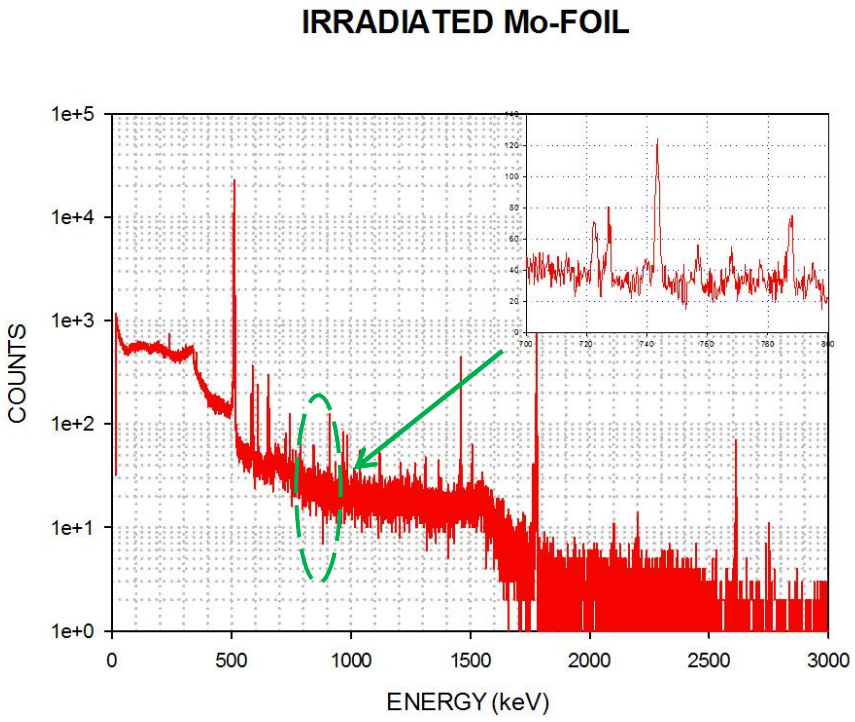

FIGURE [5.1]: Energy spectrum of neutron activated Mo-foil with many characteristic γ-rays. The inset shows visible γ-rays between 700-800keV. Data provided by Steven Lilley (CCFE).

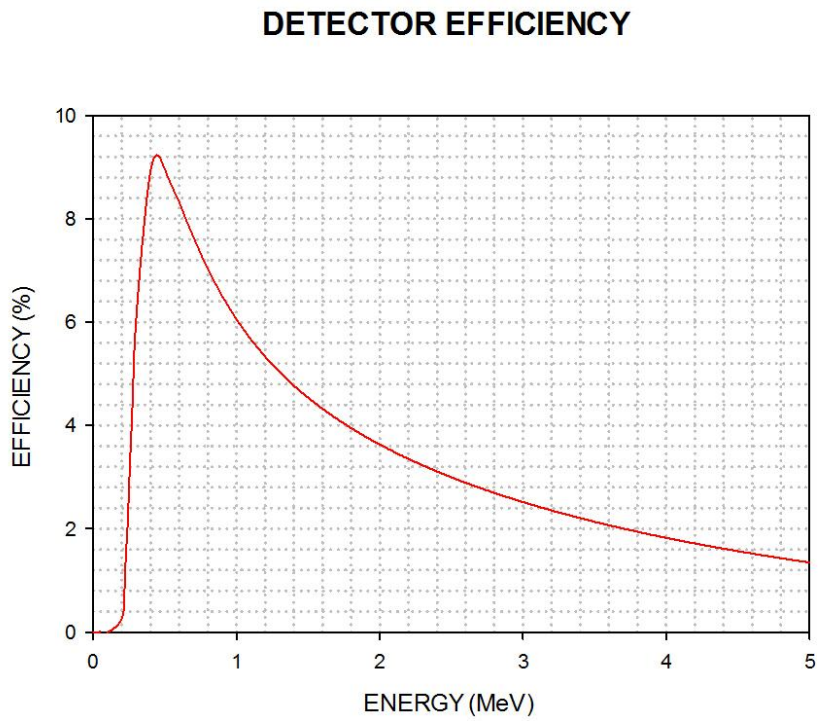

FIGURE [5.2]: Intrinsic full-energy peak efficiency fitted to equation (2.25). Data provided by Steven Lilley (CCFE).

Data from neutron activated foils were provided by Steven Lilley (CCFE). Fig. (5.1) is an energy spectrum of a molybdenum (Mo) foil weighing 0.1453g which has been neutron activated. The various energy peaks are due to the γ-rays emitted from the corresponding (n, 2n), (n, 3n), (n, p), and (n, α) reactions. The detector efficiency curve (fig. (5.2)) was obtained using calibration sources and fitted to equation (2.25), where the coefficients a_i were determined using ORTEC GammaVision v6.09 software[17] (http://www.ortec-online.com/Solutions/applications-software.aspx). Firstly in order to identify the peak, all possible products for a given reaction should be known. The products are checked on the National Nuclear Data Centre (NNDC) database (www.nndc.bnl.gov) to determine whether it is stable or unstable, and for the latter case, any characteristic γ-rays emitted. The energy peaks from the acquired spectrum are compared to those that are expected to be seen.

The stable molybdenum isotopes are ^{92}Mo, ^{94}Mo, ^{95}Mo, ^{96}Mo, ^{97}Mo, ^{98}Mo, and ^{100}Mo. Table (5.1) and fig. (5.3) below illustrates for the case of ^{98}Mo the possible nuclides produced as a result from neutron activation. For this isotope the radioactive products (the parent) are ^{98}Nb ($t_{1/2}$ = 51.3mins) which evidently decays backs to ^{98}Mo, and ^{95}Zr ($t_{1/2}$ = 64days) which initially β-decays to ^{95}Nb ($t_{1/2}$ = 86.6hrs) in turn decaying into ^{95}Mo. The reactions result in a stable form of molybdenum after irradiation however consider the case of ^{97}Mo where the (n, α) reaction produces ^{94}Zr which is stable. Since a small fraction of Mo-atoms are lost, it can be said that neutron activation is a "non-destructive technique"[5]. Although this is true for molybdenum, strictly it will depend on the target material and where it is positioned on the Segré chart.

REACTION	DAUGHTER
^{98}Mo (n, 2n) ^{97}Mo	STABLE
^{98}Mo (n, 3n) ^{96}Mo	STABLE
^{98}Mo (n, p) ^{98}Nb	^{98}Mo
^{98}Mo (n, α) ^{95}Zr	^{95}Nb

TABLE [5.1]: Isotope production for ^{98}Mo bombarded by neutrons.

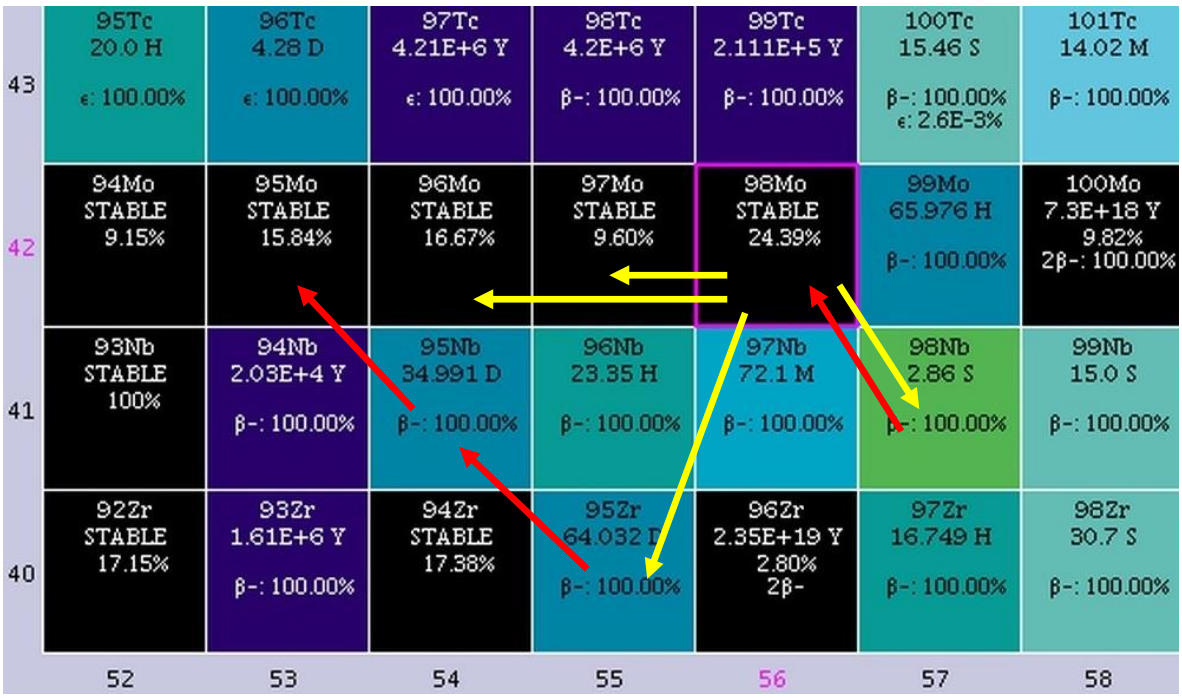

FIGURE [5.3]: Neutron activation example for ^{98}Mo. Yellow marker indicates activation pathway and red marker indicates decay pathway. Image taken from NNDC.

The photopeaks were analysed using ORTEC Meastro v6.08 software (http://www.ortec-online.com/Solutions/applications-software.aspx) to determine the number of counts detected. This was performed by highlighting a region of interest (ROI) on a given peak, the program fits the peak to a Gaussian distribution which returns information such as the peak centroid (energy), full width at half max (FWHM), and the number of counts. The energy was entered in NNDC's Nuclear Levels and Gammas Search function (http://www.nndc.bnl.gov/nudat2/indx_adopted.jsp) to identify the origin of the γ-ray. By combining equations (2.33) and (2.34) it is possible to determine the neutron cross-section σ. Rearranging equation (2.34),

$$\sigma = \frac{\lambda_Y N_c}{N_X \phi \epsilon_\gamma I_\gamma (1 - e^{-\lambda_Y t_0}) e^{\lambda_Y t_0} (e^{-\lambda_Y t_1} - e^{-\lambda_Y t_2})}$$

Consider the 726.8keV $(I_\gamma = 0.09\%)$ γ-rays from ^{98}Mo (n, p) ^{98}Nb reaction. Taking into account that the ROI yields 523 counts, ^{98}Nb has a half-life of 51.2min, a neutron flux of 3.46×10^{9}n.cm^{-2}.s^{-1}, and detector efficiency of 7.47%. The number of ^{98}Mo atoms N_X in the foil target is calculated from equation (2.33) using the information below.

FIGURE [5.4]: Isotope data for ^{98}Mo. Image taken from Periodictable.com (http://www.periodictable.com/index**).**

In turn this yields $\sigma = (1.9 \pm 0.1)$b, which is significantly larger than the published value of 5.64mb (Jendl 4.0, http://wwwndc.jaea.go.jp/jendl/j40/j40.html) shown in fig. (5.5). Applying the same procedure for the characteristic 909.6keV $(I_\gamma = 1.28\%)$ photons for the same reaction yields $\sigma = (290 \pm 20)$mb. It is closer to the value quoted by Jendl but it is still relatively large. This process was repeated with remaining identifiable peaks (see table (5.2)). Unfortunately the experimental cross-sections are not in agreement with Jendl, they are overestimated by a factor of 10 or 100 and in some case a factor of 1000. The cross-section measurements are dependent on the number of counts detected for a given photopeak. It is possible to reduce the number of counts by minimising background contribution. This can be achieved in a number of ways as mentioned in section (2.5). To observe the influence of background suppression, an anticoincidence (active) shielding system was developed at the University of York and will be discussed further in section (5.2.2).

42-Mo-98

Reaction	0.0253-eV	Maxwellian Average	g-factor	Resonance Integral	14-MeV	Fiss. Spec. Average
total	5.596 (b)	6.302 (b)	1.126	–	4.163 (b)	6.043 (b)
elastic	5.464 (b)	6.169 (b)	1.129	–	2.184 (b)	4.704 (b)
nonelastic	132.1 (mb)	132.3 (mb)	1.001	11.43 (b)	1.980 (b)	1.338 (b)
inelastic	(E-thr = 742.3 keV)				412.1 (mb)	1.319 (b)
(n,2n)	(E-thr = 8.732 MeV)				1.557 (b)	1.971 (mb)
(n,3n)	(E-thr = 15.62 MeV)				–	602.2 (nb)
(n,na)	(E-thr = 3.303 MeV)				176.1 (µb)	55.75 (nb)
(n,np)	(E-thr = 9.896 MeV)				61.40 (µb)	44.31 (nb)
(n,nd)	(E-thr = 15.80 MeV)				–	3.079e-12 (b)
capture	132.1 (mb)	132.3 (mb)	1.001	6.907 (b)	540.0 (µb)	17.51 (mb)
(n,p)	(E-thr = 3.840 MeV)				5.640 (mb)	2.722 (µb)
(n,d)	(E-thr = 7.648 MeV)				257.4 (µb)	89.05 (nb)
(n,t)	(E-thr = 9.483 MeV)				4.488 (µb)	5.073 (nb)
(n,He-3)	(E-thr = 9.627 MeV)				0.000 (b)	114.9e-15 (b)
(n,a)	0.000 (b)	0.000 (b)	–	151.2 (µb)	4.711 (mb)	8.806 (µb)
MT = 203	(E-thr = 3.840 MeV)				5.701 (mb)	2.766 (µb)
MT = 204	(E-thr = 7.648 MeV)				257.4 (µb)	89.06 (nb)
MT = 205	(E-thr = 9.483 MeV)				4.488 (µb)	5.073 (nb)
MT = 206	(E-thr = 9.627 MeV)				0.000 (b)	114.9e-15 (b)
MT = 207	0.000 (b)	0.000 (b)	–	151.2 (µb)	4.887 (mb)	8.862 (µb)

FIGURE [5.5]: Neutron cross-sections for ^{98}Mo from Jendl 4.0 database.

IDENTIFIED REACTION	ENERGY (keV)	CROSS SECTION EXPERIMENTAL (mb)	JENDL (mb)
^{95}Mo (n,p) ^{95}Nb	238.2	(3700 ± 200)	41.23
^{96}Mo (n,p) ^{96}Nb	351.6	(29000 ± 2000)	19.02
^{95}Mo (n,p) ^{95}Nb	583.0	(10300 ± 100)	41.23
^{92}Mo (n,α) ^{89}Zr	588.3	(960 ± 60)	22.98
^{96}Mo (n,p) ^{96}Nb	722.7	(83 ± 5)	19.02
^{98}Mo (n,p) ^{98}Nb	727.3	(1900 ± 100)	5.64
^{97}Mo (n,p) ^{97}Nb	743.4	(70 ± 4)	15.60
^{95}Mo (n,p) ^{95}Nb	787.8	(18000 ± 100)	41.23
^{98}Mo (n,p) ^{98}Nb	910.3	(290 ± 20)	5.64
^{100}Mo (n,p) ^{100}Nb	968.9	(1050 ± 30)	4.64
^{98}Mo (n,p) ^{98}Nb	982.7	(380 ± 20)	5.64
^{98}Mo (n,p) ^{98}Nb	1120.1	(400 ± 20)	5.64
^{92}Mo (n,2n) ^{91}Mo	1506.8	(160 ± 10)	125.30

TABLE [5.2]: Comparison of experimental neutron cross-section with Jendl.

5.2 DETECTOR DEVELOPMENT

5.2.1 HPGe & Ge(Li) CHARACTERISATION

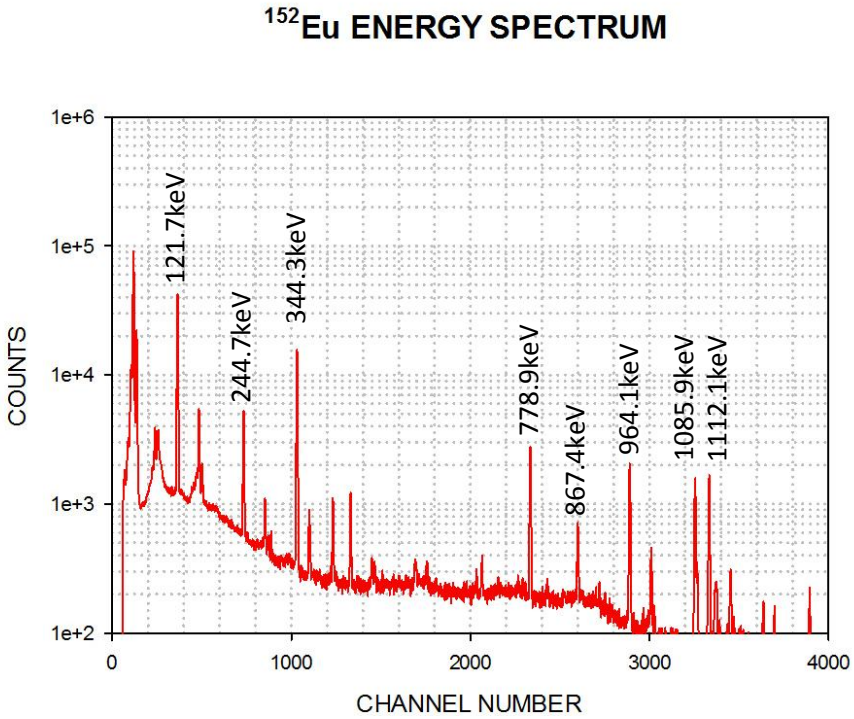

FIGURE [5.6]: ^{152}Eu spectrum acquired using the HPGe detector at CCFE.

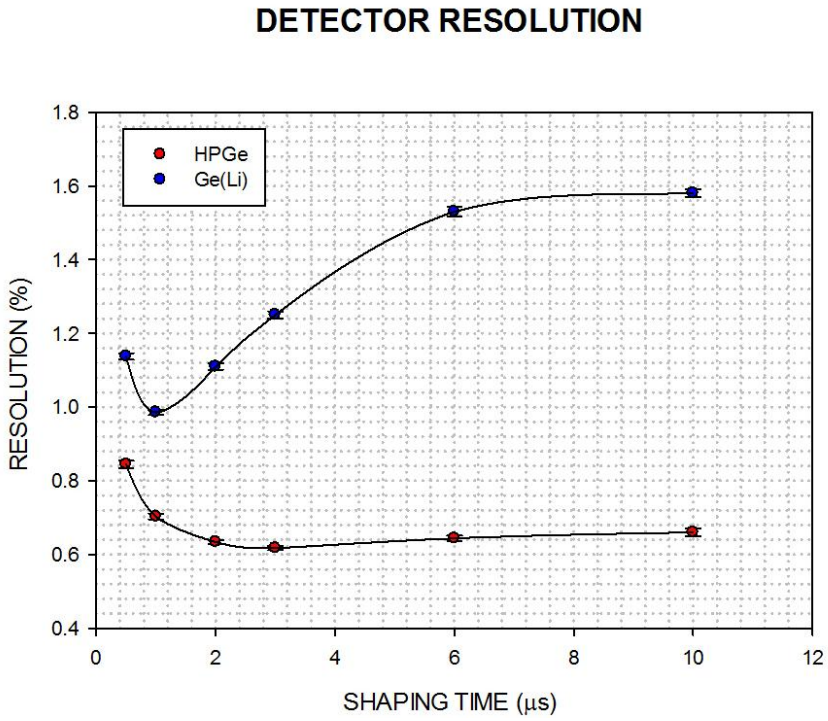

FIGURE [5.7]: Detector characterisation. The optimum shaping time was determined to be 3µs for HPGe, and 1µs for the Ge(Li) detectors.

Fig. (5.6) above is a ^{152}Eu energy spectrum. The energy resolution from the dominant 344keV $(I_\gamma = 26.5\%)$ photopeak was determined at different shaping times (fig. (5.7)), the optimum resolution occurs at 3μs. The resolution (or FWHM) is the quadrature sum of various fluctuations in the experimental setup primary from electronic noise and other factors such as statistical noise contributions[6]. The figure below shows the relationship between equivalent noise charge (ENC) and shaping time. Minimum noise occurs at a shaping time where contributions from series (thermal) and parallel (leakage current) noise are equal.

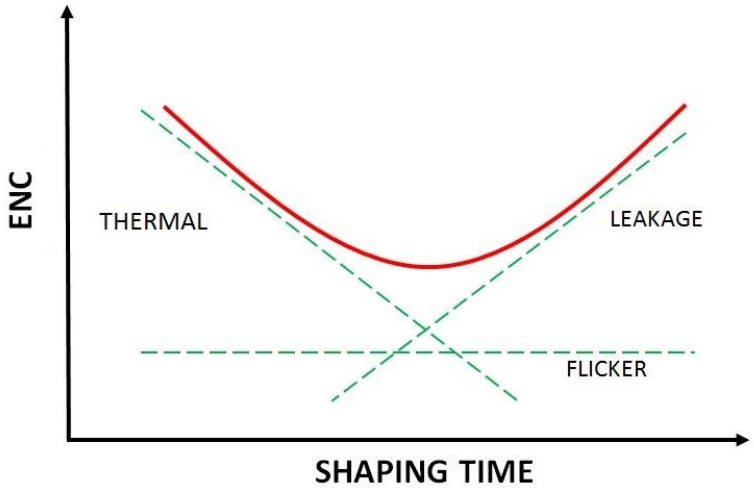

FIGURE [5.8]: Thermal (resistor) noise, leakage current (shot) noise, and flicker (1/f) noise contributions as a function of shaping time. In this example the minimum ENC occurs at the valley of the curve. Image modified from *Radiation Detection and Measurement*, G. Knoll. p632.

An energy spectrum is essentially a pulse height distribution (histogram) where events are binned into individual channels. The number of channels available is finite depending on hardware. Using calibration sources (radioisotope with known energy) the channel number can be translated into units of energy. Fig. (5.9) is a spectra of 3 calibration sources (^{241}Am, ^{133}Ba, and ^{152}Eu) illustrating a linear response between energy and channel number.

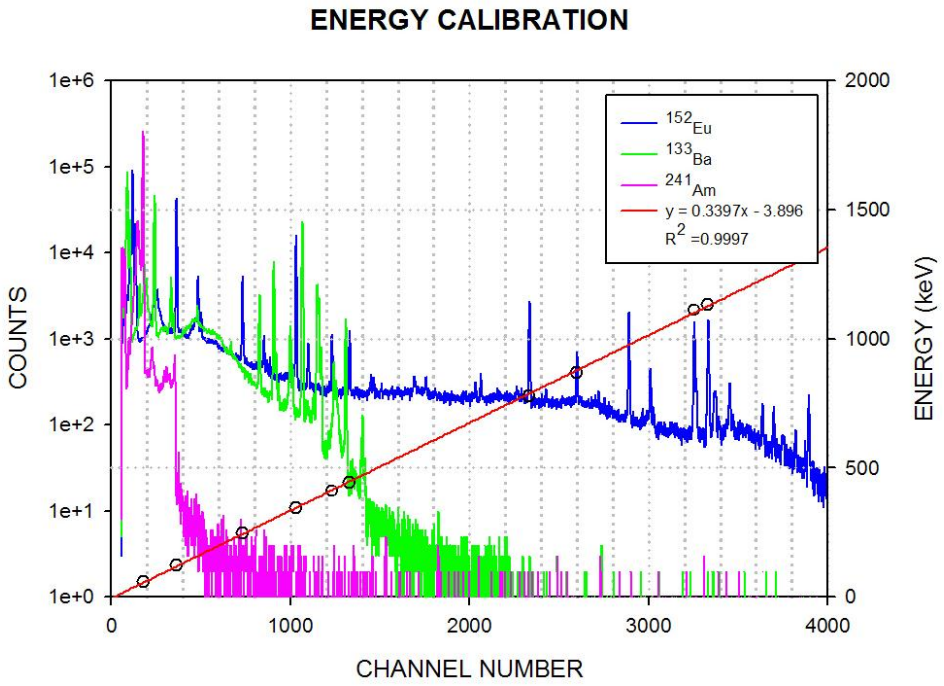

FIGURE [5.9]: Energy response of HPGe detector using calibration sources.

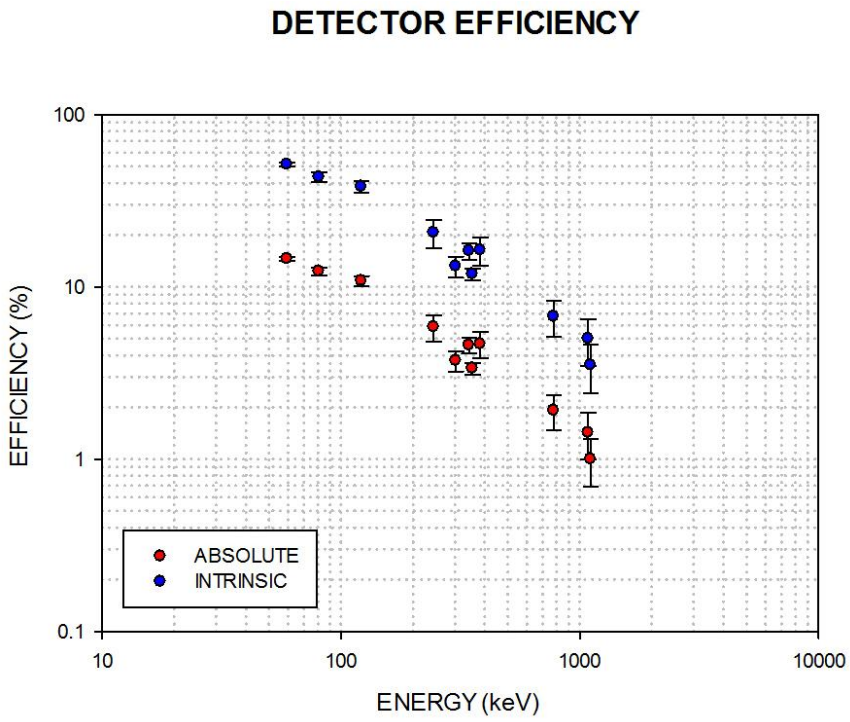

FIGURE [5.10]: Efficiency of HPGe.

Taking into account the fractional intensities of the γ-rays emitted from the radioisotope and the source-detector geometry it is possible to determine the detection efficiency of the HPGe. Fig. (5.10) above is a graph of efficiency as a function of energy. It is seen that the efficiency decreases with energy, this is because the photoelectric effect becomes less dominant at high energies (as discussed in section 4.2).

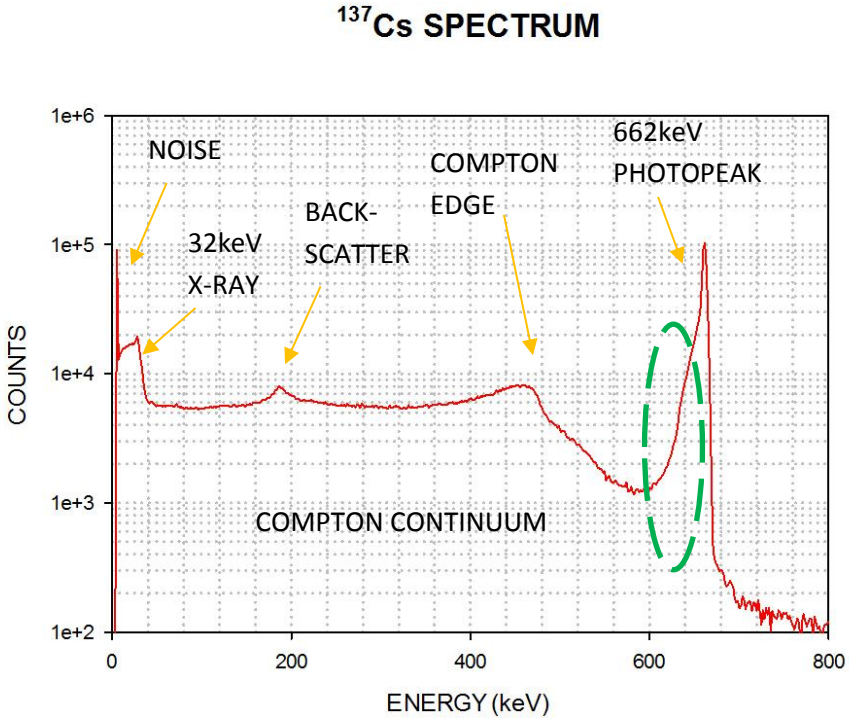

FIGURE [5.11]: ^{137}Cs calibration source acquired using Ge(Li) detector. The circled region indicates tailed feature in the photopeak due to the detector.

The figure above shows a typical energy spectrum for ^{137}Cs acquired with the Ge(Li) detector at the University of York. The spectrum illustrates various characteristic features such as the full energy 661.8keV photopeak as governed by the photoelectric effect (full energy deposition of the incident photon) which is characteristic γ-energy for ^{137}Cs. The Compton continuum relates to the photons that have scattered within the detector (partial energy deposition). The Compton edge (458.7keV) refers to the maximum energy than can be transferred to a recoil electron from a single Compton scattering event. The backscatter peak (185.1keV) is due to the detection of photons that have been scattered in the material surrounding the detector. ^{137}Cs also have characteristic X-rays via internal conversion, which results in a ^{137}Ba K_α X-ray of 32keV. A peak at low channel numbers is typically seen in an energy spectrum which is the noise (associated electronic etc.) that is picked up in the detector system[6].

As with the HPGe detector, various ^{137}Cs spectra were acquired at various shaping times (see fig. (5.7)). The performance of Ge(Li) should be on par with HPGe, however is can been seen that the resolution from the Ge(Li) is not as tight (the energy resolution is of the order of 1-2% whereas it is less than 1% for the HPGe). This could be due to the condition (age) of the detector because long term changes in charge collection efficiency can cause the detector efficiency to drift over long periods of time[6]. Ideally the photopeaks are fitted to a Gaussian distribution. The 662keV photopeak exhibit a skewed (tailing) feature caused by physical effects of the crystal such as imperfect charge collection, and escaping secondary electrons and bremsstrahlung within the active volume[6]. The tailing caused a slight issue with the Gaussian (peak) fit using the Maestro program. Incorporating the tailing in the region of interest (ROI) function led to the peak centroid to be lower than expected (registered as

657.8keV with FWHM of 20.2keV) whereas neglecting the tail the centroid was 662.9keV with FWHM of 17.1keV. Also, there were occasions where small adjustments ROI led to large variation in the resolution (e.g. FWHM ~100keV). Optimum resolution occurred with a shaping time of 1μs which was kept constant for the remainder of the project.

5.2.2 ANTICOINCIDENCE SYSTEM

The GATE input on the MCA acts as an acceptance window for the input signal. The gate signal is produced from a coincidence module (ORTEC Model 418A Universal Coincidence) using a 2nd detector (plastic BC404) in conjunction with the Ge(Li). If an event is detected in both detectors at the same time, or within a small timing window, it is said that it occurred in coincidence. In relation to the 418A, if the signals occur in the input channels at the same time then the 418A unit triggers an output to confirm that they in coincidence. To suppress background counts the system is setup such that it is in anticoincidence (in terms of electrical circuits this is a NAND gate as shown below)[18].

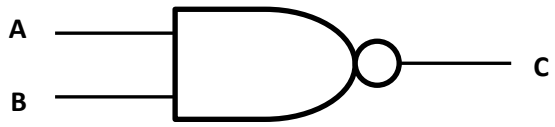

A	B	C
0	0	1
1	0	1
0	1	1
1	1	0

FIGURE [5.12]: NAND truth table. Image taken from *Techniques for Nuclear and Particle Physics Experiments*, W. Leo. p318.

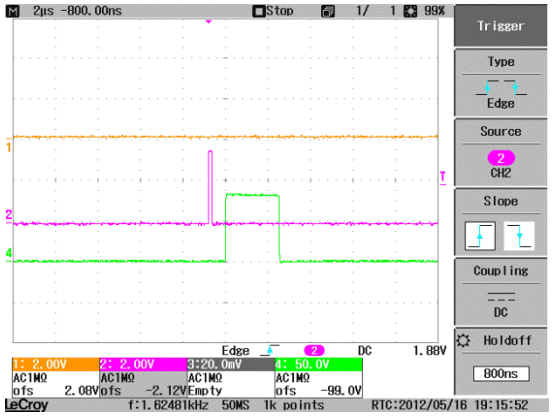

(i)

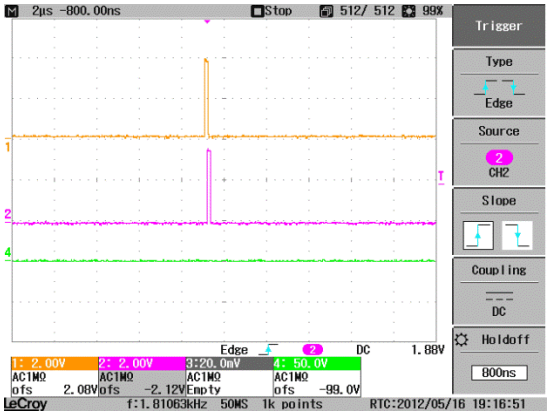

(ii)

FIGURE [5.13A]: Response observed for ORTEC 418A coincidence unit for anticoincidence counting. CH1: BC404, CH2: Ge(Li), CH4: 418A. Coincidence unit is setup such that an output is triggered constantly (i) except when the input signals occur in coincidence (ii).

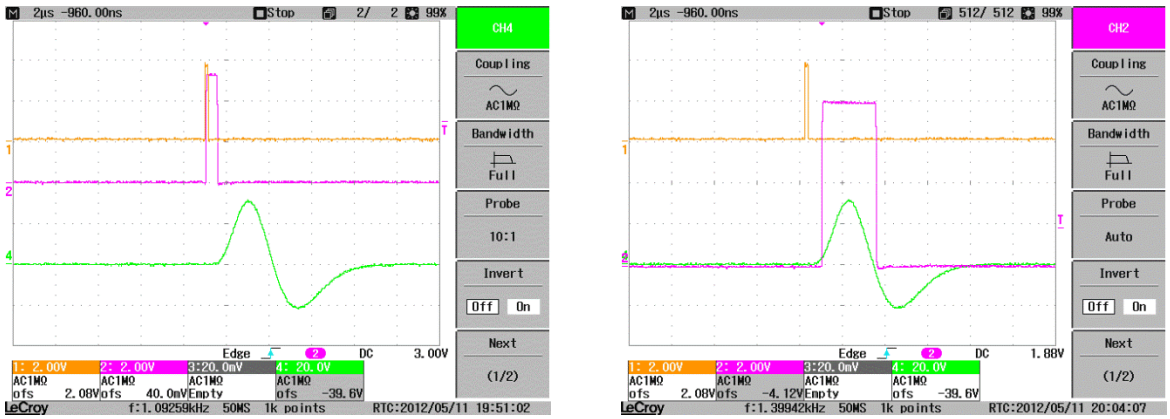

(i) (ii)

FIGURE [5.13B]: Response observed for the MCA. CH1: Ge(Li), CH2: 418A, CH4: 572. Gate window occurs before the output from the amplifier (i) so the output from 418A needs to be delayed (ii).

To check if the 418A was triggering correctly the input and output signals from the module were observed on the oscilloscope shown in fig. (5.13A). By default, with respect to the shaping amplifier (ORTEC Model 572 amplifier), the signal from the coincidence unit is triggered prematurely so a delay module was installed so the input pulses and the gate window to the MCA occur in synch with one another (fig. (5.13B)).

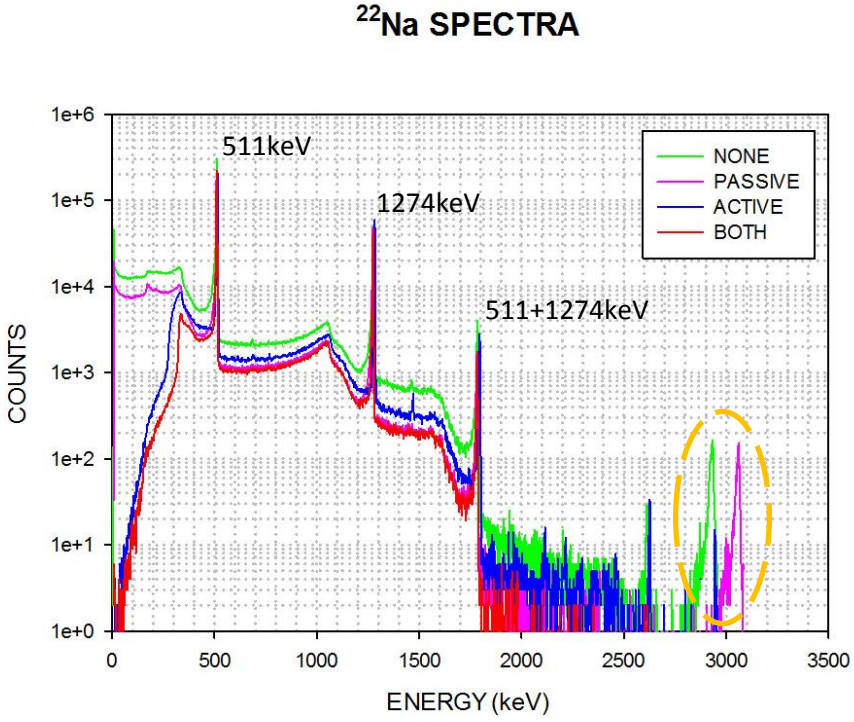

FIGURE [5.14]: Shielding comparison with lead castle and veto detector using ^{22}Na calibration source. Significant level of suppression when both passive and active shielding is employed. The circled region indicates high energy events binned in the final channel (limitation of ADC). The offset may be due to energy calibration.

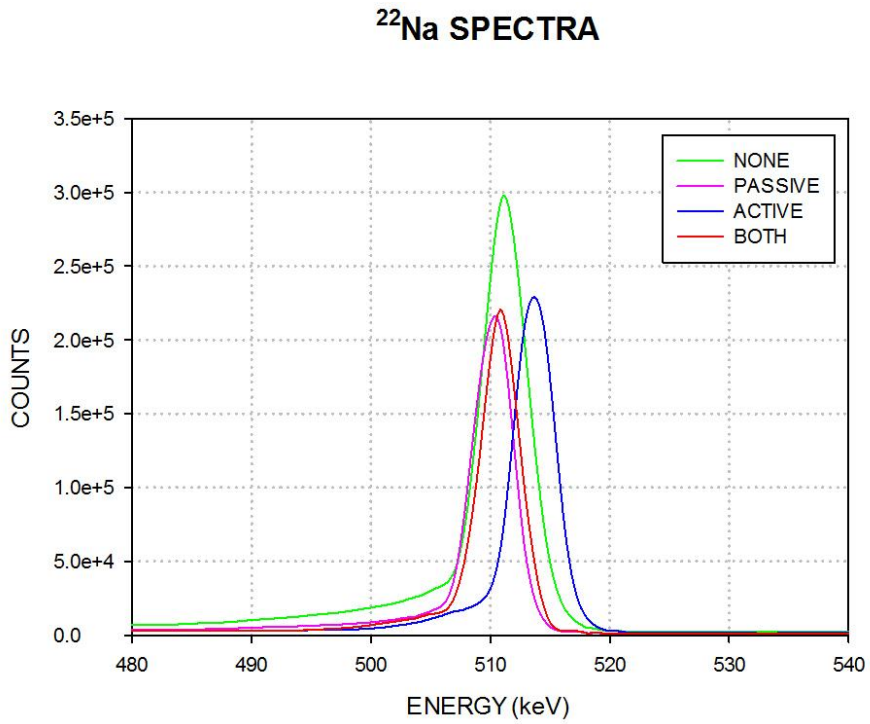

FIGURE [5.15]: Comparison of 511keV photopeak.

SHIELDING	511keV PEAK COUNTS	FWHM (keV)	1274keV PEAK COUNTS	FWHM (keV)
NONE	821790	4.65	173248	6.17
PASSIVE	453078	3.94	111352	4.17
ACTIVE	553485	3.76	144122	3.95
BOTH	448831	3.78	109470	3.91

TABLE [5.3]: Significance of background suppression.

Fig. (5.14) above illustrates various spectra to show the effects of passive and active shielding. From left to right, the 3 energy peaks refer to the characteristic 511keV and 1275keV, and the 1786keV is the summation the 2 peaks. At high count rates, accidental peaks occur from coincidences from 2 or more γ-rays from the same source which may overwhelm the number of counts of the true γ-ray peak such that the energy reflecting the sum is recorded rather than the individual energies emitted[6]. The high energy peak on the far right is referred to as the "ADC dump". Events detected with energies beyond the range of the Analogue-to-Digital Converter (ADC) are binned into the last channel. High energy cosmic or rare pile-up events may contribute towards this peak[19]. The lead castle eliminates a fraction of counts caused by low energy background radiation and any additional (calibration) sources which may be present in the laboratory. Active shielding via the plastic scintillator has significantly reduced the number of low energy counts, by rejecting pulses that occur in coincidence the photopeaks appear narrower (improved energy resolution). The combination of both passive and active shielding yields the benefits of both systems; a reduction in counts observed in photopeak with high resolution. Table (5.3) shows the counts

have reduced by 45.4% in 511keV photopeak (fig. (5.15)), and 36.8% in 1274keV photopeak. Although the spectrum in a log scale, the high energy counts (above ~2MeV) have been reduced further.

It seems that having a slab of scintillator material above the Ge(Li) detector is a crude approach to active shielding. The photopeaks in the spectrum are the main point of interest so eliminating other features would be ideal. As seen in Compton suppression systems (e.g. ORTEC CSS-P-C-3.25 Portable Compton Suppression, www.ortec-online.com/solutions) the scintillator, typically Sodium Iodide (NaI) and Bismuth Germanate (BGO), should virtually cover the germanium detector in an annular geometry. This setup is capable of suppressing coincident events from (Compton) scattered photons and background radiation, as well as escaping annihilation photons from pair production. Unfortunately this type of suppression does not perform well when measuring radioisotopes with complex decay schemes. Because many γ-rays will be emitting in coincidence it is possible that independent γ-rays can interact through both detectors and thus rejected, in turn some full energy photopeaks may be suppressed unintentionally[6].

5.3 ACTIVATION OF PAK450 ALLOY

The ultimate goal at CCFE is to produce fusion power at a commercial level. As part of the process it is important to understand how materials behave when exposed to high flux of neutrons as this will prove valuable when it comes to designing the fusion reactor.

In this section material under investigation is called PAK450. It is an alloy predominantly made up of iron (see table (5.4)). Small foil samples of the alloy, each weighing under 1g, were neutron activated at the ASP facility. As before with the metal foils, the alloy was placed in front of the HPGe detector to obtain a γ-spectrum. The dataset, provided by Steven Lilley, consists of various activation experiments labelled *EXPT92*, *EXPT93*, and *EXPT102*.

ELEMENT		%
IRON	Fe	61.1
NICKEL	Ni	14.8
CHROMIUM	Cr	17.7
MOLYBDENUM	Mo	2.57
COPPER	Cu	0.21
NITROGEN	N	0.04
CARBON	C	0.07
MANGANESE	Mn	2.86
SULPHUR	S	0.013
SILICON	Si	0.57
PHOSPHORUS	P	0.026

TABLE [5.4]: Elements in PAK alloy.

Unfortunately there was difficulty opening the saved spectrum file in Maestro. The analysis of the data was performed using RadWare[20] (radware.phy.ornl.gov). Prior to RadWare, a Fortran program *SPEC_CONV.f* was used to convert the data from ascii (*.spe) to a RadWare compliant (*.gf3) file. RadWare fits the peak using 3 components; Gaussian, skewed Gaussian, and a smoothed step-function (background). The spectrum was initially calibrated using the "*ec*" (energy calibration) command within the terminal, then energy peaks were analysed using the "*nf*" (new fit) command, in turn (similar to Maestro) this yields details such the area of the peak and its centroid as shown fig. (5.16) below. Fig. (5.17) is the efficiency curve for the PAK450 dataset.

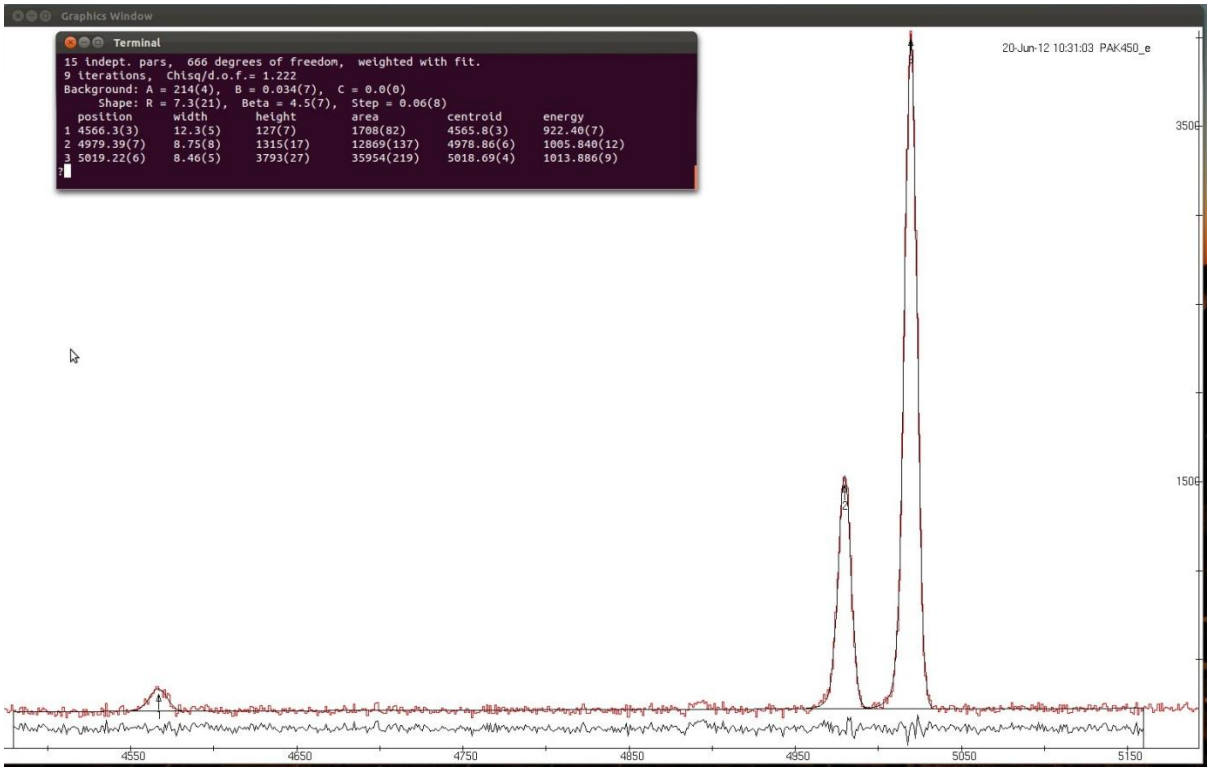

FIGURE [5.16]: Peak analysis using Radware. Selecting a region of interest for a given photopeak yields various information (and associated error) in the terminal window.

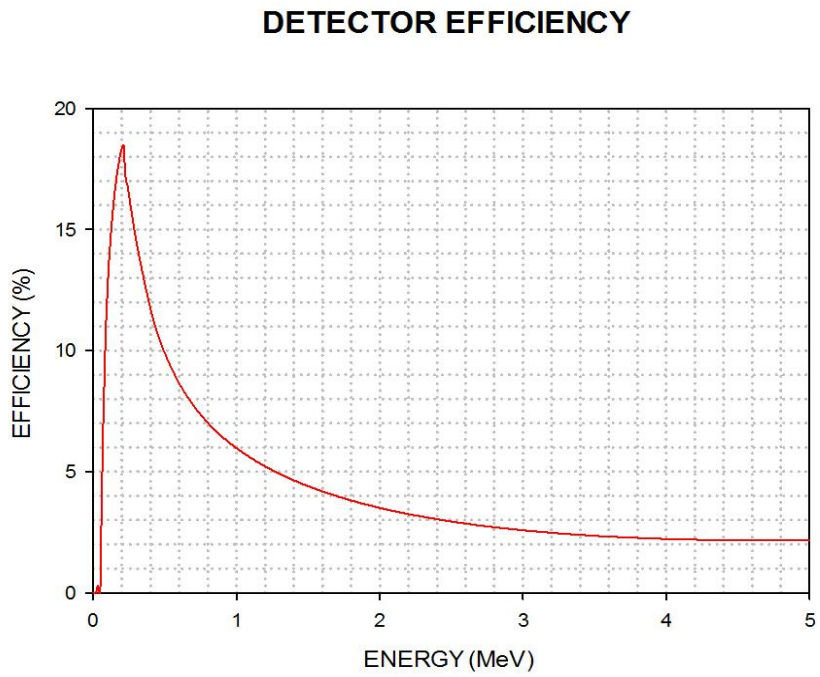

FIGURE [5.17]: Full peak efficiency for PAK450 dataset. Efficiency data fitted to equation (2.25) provided by Steven Lilley (CCFE).

ENERGY (keV)	IDENTIFIED REACTION	HALF LIFE	A_0 (Bq.g^{-1}) EXPT92	EXPT93	EXPT102
90.64	^{50}Cr (n,2n) ^{49}Cr	42.3mins	(4.7 ± 0.1)	(3.3 ± 0.1)	(3.9 ± 0.1)
121.96	^{57}Fe (n,p) ^{57}Mn	85.4sec	(1800 ± 30)	(1730 ± 30)	(1790 ± 30)
170.52	^{30}Si (n,α) ^{27}Mg	9.5mins	(18.3 ± 0.4)	(12.9 ± 0.3)	(20.8 ± 0.4)
319.57	^{53}Cr (n,3n) ^{51}Cr	27.7days	(59 ± 1)	(58 ± 1)	(53.2 ± 0.9)
352	^{57}Fe (n,p) ^{57}Mn	85.4sec	(2050 ± 70)	(1620 ± 60)	(1970 ± 71)
377	^{54}Fe (n,3n) ^{52}Fe	8.27hrs	(730 ± 20)	(850 ± 20)	-
758	^{58}Ni (n,2n) ^{57}Ni	6.01days	(17800 ± 900)	(16300 ± 900)	(17400 ± 900)
843.27	^{30}Si (n,α) ^{27}Mg	9.46mins	(22.02 ± 0.09)	(20.00 ± 0.09)	(25.1 ± 0.1)
846.27	^{56}Fe (n,p) ^{56}Mn	2.58hrs	(2020 ± 6)	(1971 ± 6)	(1670 ± 5)
922	^{57}Fe (n,p) ^{57}Mn	85.4sec	(2480 ± 60)	-	(2590 ± 60)
1005.91	^{53}Cr (n,p) ^{53}V	1.61mins	(377 ± 5)	(390 ± 5)	(360 ± 6)
1013.94	^{30}Si (n,α) ^{27}Mg	9.46mins	(19.5 ± 0.1)	(17.9 ± 0.1)	(25.4 ± 0.1)
1163	^{31}P (n,2n) ^{30}P	2.49mins	(2500 ± 80)	(2450 ± 90)	(2410 ± 90)
1172	^{60}Ni (n,p) ^{60}Co	5.27yrs	(8.5 ± 0.2)	(8.5 ± 0.1)	(8.0 ± 0.1)
1333.02	^{60}Ni (n,p) ^{60}Co	5.27yrs	(5.3 ± 0.1)	-	(6.1 ± 0.2)
1433.59	^{52}Cr (n,p) ^{52}V	3.74mins	(4070 ± 20)	(4050 ± 20)	(3870 ± 20)
1778.6	^{28}Si (n,p) ^{28}Al	2.24mins	(34.6 ± 0.3)	(34.3 ± 0.3)	(33.1 ± 0.3)
1810.41	^{56}Fe (n,p) ^{56}Mn	2.58hrs	(1620 ± 10)	(1610 ± 10)	(1370 ± 10)
2113	^{56}Fe (n,p) ^{56}Mn	2.58hrs	(1640 ± 20)	(1600 ± 20)	(1390 ± 20)
2522.9	^{56}Fe (n,p) ^{56}Mn	2.58hrs	(1640 ± 70)	(1740 ± 70)	(1620 ± 70)
2657.2	^{56}Fe (n,p) ^{56}Mn	2.58hrs	(9700 ± 200)	(9500 ± 200)	(8200 ± 200)
2751	^{64}Ni (n,α) ^{61}Fe	5.98mins	(1100 ± 70)	(1720 ± 70)	-
2959.46	^{56}Fe (n,p) ^{56}Mn	2.58hrs	(9200 ± 200)	(9300 ± 200)	(7900 ± 200)

TABLE [5.5]: Induced activity of PAK alloy.

Table (5.5) above summarises the induced activity of the alloy. It is important to note that not all energy peaks could be identified. The unknown peaks may correspond to summation of various peaks. The majority of the identified peaks originate from ^{56}Fe (91.75% abundance) because over 60% of the alloy itself is made up of iron. The purpose of the dataset is to look for consistency. In terms of reactor design it is important to observe common induced reactions as well as the induced activity; the latter case has importance in health and safety aspects with personnel who are working within close proximity of the reactor. Due to the nature of the reactor, understanding of biological effects of radiation and radiation protection is paramount to minimise unnecessary exposure to workers. Since the test foils are small, for convenience the induced activity was determined in units of Becquerels per unit mass (Bq.g^{-1}) of the alloy. Below is a general expression for the exposure rate of a given source,

$$X = \frac{\Gamma \alpha}{d^2}$$

Where Γ is the exposure rate constant of a particular source with an activity α at a distance d. From the expression above the exposure rate constant is quoted in units of Roentgens (R) per hour for a 1 curie source 1 meter away, although published values are typically quoted in units of R.cm^2.mCi^{-1}.hr^{-1} (where 1 curie (Ci) is equivalent to 3.7×10^{10}Bq)[6,18].

The Roentgen is an old unit to express the measure of exposure, which by convention, is still used today. By definition 1 Roentgen is the exposure that produces 1esu (electrostatic unit) per unit volume in air.

$$1R = 2.58 \times 10^{-4}\ \text{C.kg}^{-1}$$

$$\sim 1.61 \times 10^{15}\ \text{ion-pairs.kg}^{-1}.$$

The average energy to create an ion-electron pair (referred as the W-value) in air is 33.7eV.

$$\therefore 1R \sim 5.42 \times 10^{10}\ \text{MeV.kg}^{-1}.$$

Taking into account that 1MeV is equivalent to 1.6×10^{-13}J, photons having a radiation weighting (quality) factor of 1, and by definition the absorbed dose is the energy absorbed per unit mass, it is possible to express the exposure rate (strictly this becomes the dose-rate, DR) in units of Sieverts (Sv) per hour in air[6,7,18].

Consider the 90.6keV photopeak (*EXPT92*) observed from the ^{50}Cr(n, 2n)^{49}Cr reaction with an induced activity of 4.7Bq (equivalent to 1.27×10^{-10}Ci). The exposure rate constant for ^{49}Cr is 5.95R.cm^2.mCi^{-1}.hr^{-1} [21], in turn the exposure rate becomes 7.55×10^{-11}R.hr^{-1} at 1m. Taking into account that 1R ~ 8.67×10^{-3}J.kg^{-1} in air then the ^{49}Cr radionuclide yields a dose-rate of 6.55×10^{-13}Sv.hr^{-1}.

ENERGY (keV)	IDENTIFIED REACTION	$\Gamma^{\#}$ (R.cm^2.mCi^{-1}.hr^{-1})	X (R.hr^{-1}) EXPT92	EXPT93	EXPT103
90.64	^{50}Cr (n,2n) ^{49}Cr	5.95	7.55×10^{-11}	5.33×10^{-11}	6.29×10^{-11}
121.96	^{57}Fe (n,p) ^{57}Mn	0.51	2.49×10^{-9}	2.39×10^{-9}	2.49×10^{-9}
170.52	^{30}Si (n,α) ^{27}Mg	4.89	2.41×10^{-10}	1.70×10^{-10}	2.75×10^{-10}
319.57	^{53}Cr (n,3n) ^{51}Cr	0.178	2.87×10^{-11}	2.80×10^{-11}	2.56×10^{-11}
352	^{57}Fe (n,p) ^{57}Mn	0.51	2.83×10^{-9}	2.24×10^{-9}	2.72×10^{-9}
377	^{54}Fe (n,3n) ^{52}Fe	4.12	1.40×10^{-8}	1.65×10^{-8}	-
758	^{58}Ni (n,2n) ^{57}Ni	9.93	4.79×10^{-7}	4.37×10^{-7}	4.72×10^{-7}
843.27	^{30}Si (n,α) ^{27}Mg	4.89	2.91×10^{-10}	2.64×10^{-10}	3.31×10^{-10}
846.27	^{56}Fe (n,p) ^{56}Mn	8.54	4.66×10^{-8}	4.55×10^{-8}	3.85×10^{-8}
922	^{57}Fe (n,p) ^{57}Mn	0.51	3.08×10^{-7}	-	3.67×10^{-7}
1005.91	^{53}Cr (n,p) ^{53}V	5.57	5.68×10^{-9}	5.90×10^{-9}	5.43×10^{-9}
1013.94	^{30}Si (n,α) ^{27}Mg	4.89	2.58×10^{-10}	2.37×10^{-10}	3.36×10^{-10}
1163	^{31}P (n,2n) ^{30}P	5.87	4.04×10^{-8}	3.89×10^{-8}	3.82×10^{-8}
1172	^{60}Ni (n,p) ^{60}Co	12.9	2.99×10^{-10}	2.99×10^{-10}	2.81×10^{-10}
1333.02	^{60}Ni (n,p) ^{60}Co	12.9	1.84×10^{-10}	-	2.11×10^{-10}
1433.59	^{52}Cr (n,p) ^{52}V	7.21	7.94×10^{-8}	7.89×10^{-8}	7.54×10^{-8}
1778.6	^{28}Si (n,p) ^{28}Al	8.37	7.83×10^{-10}	7.75×10^{-10}	7.49×10^{-10}
1810.41	^{56}Fe (n,p) ^{56}Mn	8.54	3.73×10^{-8}	3.72×10^{-8}	3.15×10^{-8}
2113	^{56}Fe (n,p) ^{56}Mn	8.54	3.78×10^{-8}	3.70×10^{-8}	3.21×10^{-8}
2522.9	^{56}Fe (n,p) ^{56}Mn	8.54	3.79×10^{-8}	4.01×10^{-8}	3.74×10^{-8}
2657.2	^{56}Fe (n,p) ^{56}Mn	8.54	2.23×10^{-7}	2.19×10-^{7}	1.89×10^{-7}
2751	^{64}Ni (n,α) ^{61}Fe	7.18	2.14×10^{-8}	3.35×10^{-8}	-
2959.46	^{56}Fe (n,p) ^{56}Mn	8.54	2.11×10^{-7}	2.15×10^{-7}	1.83×10^{-7}

TABLE [5.6]: Exposure rate (R.hr^{-1}) at a distance of 1m. $^{\#}$ Exposure rate constant taking from a paper by Smith and Stabin[21].

Table (5.6) indicates the exposure rate (at 1m) of the irradiated alloy. Table (5.7) is an example of the possible dose rate (in air) for the *EXPT92* dataset. The overall dose-rate (from the identified γ-rays) is 13.4nSv.hr^{-1} which at first glance is considered low since the average UK annual background radiation dose is 2.7mSv, and the annual limit for employees in the nuclear industry is 20mSv[22]. From these findings a continuous exposure of over 170 years would result in the annual dose limit for classified workers. However it should be taken into account that these results are based on 1g test sample (which was irradiated for 5 minutes) at a distance of 1m in air, whereas, the fusion reactor will be operating (irradiating) over a significantly long period of time. It also does not take into account other materials surrounding the reactor which may affect the exposure rate. It would be interesting to use dosimeters order to obtain accurate results.

ENERGY (keV)	IDENTIFIED REACTION	DOSE-RATE ($pSv.hr^{-1}$)
90.64	^{50}Cr (n,2n) ^{49}Cr	0.7
121.96	^{57}Fe (n,p) ^{57}Mn	21.6
170.52	^{30}Si (n,α) ^{27}Mg	2.1
319.57	^{53}Cr (n,3n) ^{51}Cr	0.2
352	^{57}Fe (n,p) ^{57}Mn	24.5
377	^{54}Fe (n,3n) ^{52}Fe	121.7
758	^{58}Ni (n,2n) ^{57}Ni	4150.6
843.27	^{30}Si (n,α) ^{27}Mg	2.5
846.27	^{56}Fe (n,p) ^{56}Mn	404.3
922	^{57}Fe (n,p) ^{57}Mn	2670.6
1005.91	^{53}Cr (n,p) ^{53}V	49.3
1013.94	^{30}Si (n,α) ^{27}Mg	2.2
1163	^{31}P (n,2n) ^{30}P	350.1
1172	^{60}Ni (n,p) ^{60}Co	2.6
1333.02	^{60}Ni (n,p) ^{60}Co	1.6
1433.59	^{52}Cr (n,p) ^{52}V	688.3
1778.6	^{28}Si (n,p) ^{28}Al	6.8
1810.41	^{56}Fe (n,p) ^{56}Mn	323.5
2113	^{56}Fe (n,p) ^{56}Mn	328.1
2522.9	^{56}Fe (n,p) ^{56}Mn	329.0
2657.2	^{56}Fe (n,p) ^{56}Mn	1933.3
2751	^{64}Ni (n,α) ^{61}Fe	185.4
2959.46	^{56}Fe (n,p) ^{56}Mn	1829.4

TABLE [5.7]: Potential dose rate of PAK alloy (*EXPT92*) at 1m in air. The sum dose-rate is 13.4nSv.hr^{-1}.

6. CONCLUSION

Neutron Activation Analysis is main nuclear technique employed in this project. For simplicity, a sample that has been neutron activated results in emission of characteristic γ-rays. At the ASP facility the target foils were irradiated for 5 minutes and then placed in front of a HPGe detector to acquire and γ-spectrum of the activated sample. Analysis of irradiated molybdenum foils resulted in neutron cross-section measurements were larger than published values (Jendl-4.0) by a factor of 100 or more. The cross-section measurements are proportional to the number of counts detected so background suppression is an approach to increase the precision of experimental measurements.

Passive shielding is the simple route by constructing a lead castle to surround the detector. This can significantly reduce the low energy background contribution however presence of high energy cosmic rays (~MeV) can penetrate through the lead castle and interact with the detector. Active shielding employs a secondary detector to veto events that occur in coincidence (interaction in both detectors at the same time). An anticoincidence system was developed at the University of York using a Ge(Li) detector with a plastic BC404 scintillator acting as the veto detector. A scintillator is typically used as the secondary detector as they are generally faster and more efficient that their semiconductor (HPGe/Ge(Li)) counterpart albeit at the cost of (energy) resolution. From experiments using ^{22}Na calibration (γ = 511, 1274keV) source it was found that passive shielding alone resulted in significant reduction in count-rate. Active shielding also reduced the count-rate (not as much as passive shielding) and there was a slight improvement in resolution (FWHM reduced by a few keV). Employing both passive and active shielding combines the benefits as a single system, the 511keV and 1274keV photopeaks saw a reduction in counts of 45.4% and 36.8% respectively.

PAK450 (an alloy predominantly made of iron) is a potential material of interest. Various datasets of the irradiated PAK foils were analysed to observe for reoccurring reactions and induced activity of the foils. By referring to published values of exposure rate constants for a given source it is possible to determine the exposure rate of the radionuclide. This information can be converted into meaningful units such as the dose-rate which has great importance in terms of health physics. From the identified γ-rays, the total dose-rate from the *EXPT92* sample was 13.4nSv.hr^{-1} in air at 1m. Further work needs to be carried out to validate these dose-rates.

FURTHER INVESTIGATIONS

FLUKA is not as well-known as other programs such as GEANT-4 and MCNP so comparison of Monte-Carlo simulation may be useful. FLUKA is praised for its easy user friendly interface using the card-based commands unfortunately this means the user will be confined within the card system depending on experience. If the user requires something not predefined or more advanced then it requires coding outside of FLUKA.

After setting up and testing the active shielding at the University of York, it would be useful to transport the detector to CCFE/ASP to observe the performance of the veto detector onsite. Through further funding it may be interesting to invest in large volume scintillators to observe the significance of surrounding the HPGe/Ge(Li) detector (or even the possibility of investing in a commercial Compton suppression system). Installing an array of Ge-detectors may be beneficial as this would increase the detection field of view. It would also be interesting to investigate in other scintillation materials (e.g. Lanthanum Bromide).

From the analysis of the irradiated PAK alloy, further work in dosimetry and aspects in radiation protection will be beneficial for the health and safety of personnel and visitors.

7.REFERENCES

1. CULHAM CENTRE FOR FUSION ENERGY www.ccfe.ac.uk
2. INTERNATIONAL ATOMIC ENERGY AGENCY *Power Reactor Information system* http://www.iaea.org/PRIS/home.aspx
3. ITER www.iter.org
4. KRANE, K. S. (1988) *Introductory Nuclear Physics.* 2nd Ed. John Wiley & Sons, Inc., USA.
5. LILLEY, J. (2001) *Nuclear Physics, Principles and Applications.* John Wiley & Sons Ltd, UK.
6. KNOLL, G. F (2000) *Radiation Detection and Measurement.* 3rd Ed. John Wiley & Sons, Inc. USA.
7. MARTIN, J. (2006) *Physics for Radiation Protection, A Handbook.* 2nd Ed. Wiley-VCH Verlag GmbH & Co., Germany.
8. ORTEC, INC. (2009) *High-Purity Germanium (HPGe) Detector Manufacturing*. http://www.ortec-online.com/download/High-Purity-Germanium-HPGe-Detector-Manufacturing.pdf
9. KNIEST, F. Saint-Gobain Crystals (Holland Office). Private communication, 11/05/2012.
10. UNIVERSITY OF SURREY (2008) *REP2: Gamma-Ray Spectroscopy*. Lab script.
11. EBY, N (2007) *Instrumental Neutron Activation Analysis*. University of Massachusetts. http://serc.carleton.edu/research_education/geochemsheets/techniques/INAA.html
12. BATTISTONI, G, MURARO, S., SALA, P. R, CERUTTI, F., FERRARI, A., ROESLER, S., FASSO, A. & RANFT, J *The FLUKA code: Description and benchmarking.* Proceedings of the Hadronic Shower Simulation Workshop 2006, Fermilab 6--8 September 2006, M. Albrow, R. Raja eds., AIP Conference Proceeding 896, 31-49, (2007)
13. FERRARI, A., SALA, P. R., FASSO, A. & RANFT, J. *FLUKA: a multi-particle transport code.* CERN-2005-10 (2005), INFN/TC_05/11, SLAC-R-773
14. VLACHOUDIS, V. *Flair FLUKA Advanced Interface*. CERN 2006.
15. PORTA, A. A., CAMPI, F. *Simulation of an HPGe Detector and Marinelli's Beaker source to derive Efficiency Curves with FLUKA 2005.6* Nuclear Engineering Department. CeSNEF. Polytechnic of Milan. www.fluka.org/web_archive/earchive/prova/att-1433/Example-HPGe.doc
16. WURTH, S. (2008) *RE: DETECT, recovering the output.* FLUKA Discussion Forum http://www.fluka.org/web_archive/earchive/prova/1396.html
17. LILLEY, S., PACKER, L., GILBERT, M., & PAMPIN, R. (2011) *Summary of initial experimental activities at the ASP 14MeV neutron irradiation facility*. Culham Centre for Fusion Energy.
18. LEO, W. R. (1994) *Techniques for Nuclear and Particle Physics Experiments* 2nd Ed. Springer-Verlag, Germany.

19. JOSHI, P. University of York. Private communication, 30/10/12.
20. RADFORD, D. *RadWare*. Oak Ridge National Laboratory, USA. http://radware.phy.ornl.gov/
21. SMITH, D. S. & STABIN, M. G. (2012) *Exposure Rate Constants and Lead Shielding for over 1100 Radionuclides*. Health Physics Society. March 2012 – Volume 102 – Issue 3 p271-291.
22. HEALTH PROTECTION AGENCY (2012) *Dose Comparisons for Ionising Radiation*. http://www.hpa.org.uk/Topics/Radiation/UnderstandingRadiation/UnderstandingRadiationTopics/DoseComparisonsForIonisingRadiation/

APPENDIX 1. HPGe SCHEMATIC

GERMANIUM DETECTOR DIAGRAM

SERIAL NUMBER 27-N1847B

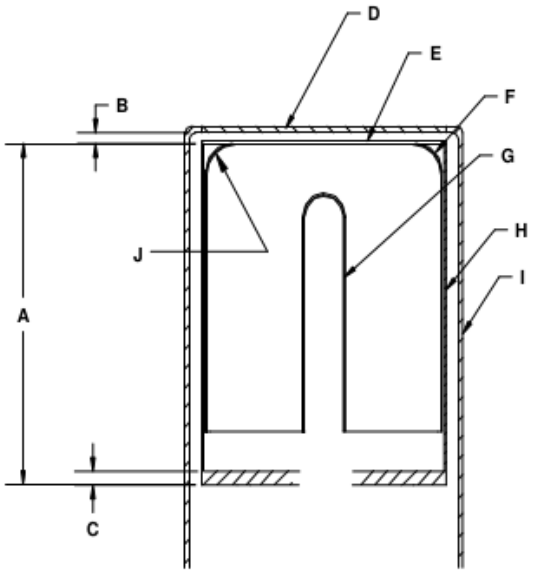

COMPANY PRIVATE

BASIC DETECTOR DIMENSIONS	
DETECTOR DIAMETER	50.1 mm
DETECTOR LENGTH	56.4 mm
DETECTOR END RADIUS (J)	8 mm, NOMINAL
HOLE DIAMETER	10.4 mm
HOLE DEPTH	48.3 mm
HOLE BOTTOM RADIUS	HOLE DIAMETER / 2, NOMINAL

MISCELLANEOUS DETECTOR ASSEMBLY DIMENSIONS AND MATERIALS			
IDENTIFIER	DIMENSION	DESCRIPTION	MATERIAL(S)
A	94 mm	MOUNT CUP, LENGTH	ALUMINUM
B	3 mm	END CAP TO CRYSTAL GAP	N.A.
C	3.2 mm	MOUNT CUP BASE	ALUMINUM
D	0.5 mm	END CAP WINDOW	BERYLLIUM
E	0.05 mm	INSULATOR/SHIELD	ALUMINIZED MYLAR
F	0.3 microns	OUTSIDE CONTACT LAYER	Ge with Boron ions
G	700 microns	HOLE CONTACT LAYER	Ge with Lithium ions
H	0.76 mm	MOUNT CUP WALL	ALUMINUM
I	1.3 mm	END CAP WALL	ALUMINUM

ORTEC
801 S. ILLINOIS AVE.
OAK RIDGE TN 37831

FIGURE [A1]: Schematic of HPGe detector. Datasheet courtesy of Steven Lilley (Culham Centre for Fusion Energy).

APPENDIX 2. LabHPGe.inp (FLAIR INPUT FILE)

```
TITLE

* Set the defaults for precision simulations
DEFAULTS
PRECISIO
* Define the beam characteristics
BEAM       -.0011121             10000.0       0.1       0.1
PHOTON
* Define the beam position
BEAMPOS          0.0      27.0       0.0
*PHYSICS           2.
EVAPORAT
GEOBEGIN
COMBNAME
    0    0
* Black body
SPH blkbody    0.0 0.0 0.0 100000.0
* Void sphere
SPH void       0.0 0.0 0.0 10000.0
* Steel Base
RPP Base       -27.5 27.5 0.0 1.0 -17.0 23.0
* Lead Castle
RPP PbCastle   -20. 20. 1.0 41.0 -12.0 18.0
* Steel Liner 1
RPP Liner1     -15.0 15.0 1.0 41.0 -8. 13.
* Steel Liner 2
RPP Liner2     -20.0 -6.0 1.0 41.0 -12.0 -11.0
* Steel Liner 3
RPP Liner3     6.0 20.0 1.0 41.0 -12.0 -11.0
* Steel Liner 4
RPP Liner4     -7.0 -6.0 1.0 41.0 -11.0 -8.0
* Steel Liner 5
RPP Liner5     6.0 7.0 1.0 41.0 -11.0 -8.0
* Cavity in Lead Castle
RPP Cavity1    -14.0 14.0 1.0 41.0 -7.0 12.0
* Cavity between Castle and Door
RPP Cavity2    -6.0 6.0 1.0 41.0 -12.0 -7.0
* Door Liner
RPP Door1      -13.0 13.0 0.0 41.0 -18.0 -12.0
* Lead Door
RPP Door2      -12.5 12.5 0.0 41.0 -17.5 -12.5
* Source Holder Al-can
RCC Holder1    0.0 27.8 0.0 0.0 10.2 0.0 4.25
* Source Holder Cavity
RCC Holder2    0.0 28.0 0.0 0.0 10. 0.0 3.25
* Perspex Base
RCC Holder3    0.0 25.8 0.0 0.0 2.0 0.0 4.25
* Perspex Cavity
RCC Holder4    0.0 26.8 0.0 0.0 1.2 0.0 2.3
* External Al-Mounting Can
RCC Det1       0.0 28.0 0.0 0.0 14.0 0.0 3.01103
* Mounting Can Cavity
RCC Det2       0.0 28.0 0.0 0.0 13.5 0.0 2.88103
* Al-End Cap Window
RCC Det3       0.0 28.0 0.0 0.0 0.05 0.0 2.88103
```

```
* Inner Al-Mounting Cup
RCC Det4       0.0 28.35 0.0 0.0 9.4 0.0 2.58103
* Inner Mounting Cavity
RCC Det5       0.0 28.35 0.0 0.0 9.08 0.0 2.50503
* Mylar Insulator
RCC Det6       0.0 28.35 0.0 0.0 0.005 0.0 2.50503
* Outer Boron Ion
RCC BorOut5    0.0 29.2 0.0 0.0 4.84 0.0 2.5053
* Ge-crystal
RCC Ge5        0.0 29.2 0.0 0.0 4.84 0.0 2.505
* Inner Lithium Ions
RCC Lith5      0.0 29.31 0.0 0.0 4.73 0.0 0.59
* "Inner Finger"
RCC Hole5      0.0 29.41 0.0 0.0 4.63 0.0 0.52
* Boron Bulletized Face
TRC BorOut1    0.0 28.4 0.0 0.0 0.0609 0.0 1.7053 2.0114
* Boron Bulletized Face
TRC BorOut2    0.0 28.4609 0.0 0.0 0.1734 0.0 2.0114 2.2703
* Boron Bulletized Face
TRC BorOut3    0.0 28.6343 0.0 0.0 0.2596 0.0 2.2703 2.4413
* Boron Bulletized Face
TRC BorOut4    0.0 28.8939 0.0 0.0 0.3061 0.0 2.4413 2.5053
* Ge Bulletized Face
TRC Ge1        0.0 28.4003 0.0 0.0 0.0609 0.0 1.705 2.0111
* Ge Bulletized Face
TRC Ge2        0.0 28.4609 0.0 0.0 0.1734 0.0 2.0111 2.27
* Ge Bulletized Face
TRC Ge3        0.0 28.6343 0.0 0.0 0.2596 0.0 2.27 2.441
* Ge Bulletized Face
TRC Ge4        0.0 28.8939 0.0 0.0 0.3061 0.0 2.441 2.505
* Bulletized Lithium Face
TRC Lith1      0.0 29.14 0.0 0.0 0.015224 0.0 0.39 0.466536
* Bulletized Lithium Face
TRC Lith2      0.0 29.155224 0.0 0.0 0.043355 0.0 0.466536 0.531421
* Bulletized Lithium Face
TRC Lith3      0.0 29.198579 0.0 0.0 0.064885 0.0 0.531421 0.574776
* Bulletized Lithium Face
TRC Lith4      0.0 29.263464 0.0 0.0 0.076536 0.0 0.574776 0.59
* Hole Bulletized Face
TRC Hole1      0.0 29.21 0.0 0.0 0.01522 0.0 0.32 0.39654
* Hole Bulletized Face
TRC Hole2      0.0 29.22522 0.0 0.0 0.04334 0.0 0.39654 0.46142
* Hole Bulletized Face
TRC Hole3      0.0 29.26856 0.0 0.0 0.0649 0.0 0.46142 0.50478
* Hole Bulletized Face
TRC Hole4      0.0 29.33346 0.0 0.0 0.07654 0.0 0.50478 0.52
END
* Black hole
BLKBODY      5 +blkbody -void
* Void around
VOID         5 +void -Base -PbCastle -Door1 -Door2 -Det1
* Target
BASE         5 +Base -Door1 -Door2
CASTLE       5 +PbCastle -Liner1 -Liner2 -Liner3 -Liner4 -Liner5 -
Cavity1-Cavity2
LINER1       5 +Liner1 -Cavity1-Cavity2
LINER2       5 +Liner2
LINER3       5 +Liner3
```

```
LINER4        5 +Liner4
LINER5        5 +Liner5
CAVITY1       5 +Cavity1 -Holder1 -Holder2 -Holder3 -Holder4 -Det1 -Det2
CAVITY2       5 +Cavity2
DOOR1         5 +Door1 -Door2
DOOR2         5 +Door2
HOLDER1       5 +Holder1 -Holder2 -Holder4 -Det1
HOLDER2       5 +Holder2 -Holder4 -Det1 -Det2
HOLDER3       5 +Holder3 -Holder4
HOLDER4       5 +Holder4
DET1          5 +Det1 -Det2
DET2          5 +Det2 -Det3  -Det4
DET3          5 +Det3
DET4          5 +Det4 -Det5
DET5          5 +Det5 -Det6-BorOut1 -BorOut2 -BorOut3 -BorOut4 -BorOut5
DET6          5 +Det6
BOROUT1       5 +BorOut1 -Ge1
BOROUT2       5 +BorOut2 -Ge2
BOROUT3       5 +BorOut3 -Ge3
BOROUT4       5 +BorOut4 -Ge4
BOROUT5       5 +BorOut5 -Ge5
GE1           5 +Ge1
GE2           5 +Ge2
GE3           5 +Ge3
GE4           5 +Ge4-Lith1-Lith2 -Lith3 -Lith4
GE5           5 +Ge5 -Lith1 -Lith2 -Lith3 -Lith4 -Lith5
LITH1         5 +Lith1 -Hole1 -Hole2 -Hole3 -Hole4
LITH2         5 +Lith2 -Hole1 -Hole2 -Hole3 -Hole4
LITH3         5 +Lith3 -Hole1 -Hole2  -Hole3 -Hole4
LITH4         5 +Lith4 -Hole1 -Hole2 -Hole3  -Hole4 -Hole5
LITH5         5 +Lith5 -Hole1 -Hole2 -Hole3 -Hole4 -Hole5
HOLE1         5 +Hole1
HOLE2         5 +Hole2
HOLE3         5 +Hole3
HOLE4         5 +Hole4
HOLE5         5 +Hole5
END
GEOEND
MATERIAL          24.   51.9961      7.18
CHROMIUM
* Stainless-Steel (typical)
* Stainless-Steel is produced with Cr content ranging from
* 4 - 19 Atomic Percent, and with C content from 0 - 4 percent.
MATERIAL                               8.0
Stainles
COMPOUND        18.0  CHROMIUM      74.0      IRON       8.0
NICKELStainles
* 223 Lucite, Perspex
* Chemical           H    CH
* Formula            |    | 3
*               ----- C -- C -----
*                     |    |
*                     H    C - O - CH
*  C  H  O                 ||        3
*   5  8  2               O
MATERIAL                               1.19
Polymeth
```

```
COMPOUND         8.0  HYDROGEN       5.0    CARBON       2.0
OXYGENPolymeth
* Mylar, Melinex
* Chemical Formula :  H-C = C-H            H   H
*                     /       \            |   |
*       ---- O - C - C         C - C - O - C - C -------
*                 ||   \\     //    ||      |   |
*  C  H 0         O    H-C - C-H    O       H   H
*   10 8 4
MATERIAL                            1.397
Mylar
COMPOUND         8.0  HYDROGEN      10.0    CARBON       4.0
OXYGENMylar
MATERIAL          5.    10.811      2.37
BORON
MATERIAL         32.     72.61     5.323
GERMANIU
MATERIAL          3.     6.941     0.534
LITHIUM
MAT-PROP                             40.0   LITHIUM
MAT-PROP        10.0                        LITHIUM
DPA-ENER
STERNHEI      3.1221    0.1304    1.6397   0.95136    2.4993
0.14LITHIUM
MAT-PROP                            350.0  GERMANIU
MAT-PROP        20.0                        GERMANIU
DPA-ENER
STERNHEI      5.1411    0.3376    3.6096   0.07188    3.3306
0.14GERMANIU
MAT-PROP                             76.0     BORON
STERNHEI      2.8477    0.0305    1.9688   0.56224    2.4512
0.14BORON
*
..+....1....+....2....+....3....+....4....+....5....+....6....+....7..
ASSIGNMA    BLCKHOLE   BLKBODY
ASSIGNMA         AIR      VOID
ASSIGNMA    Stainles      BASE
ASSIGNMA        LEAD    CASTLE
ASSIGNMA    Stainles    LINER1
ASSIGNMA    Stainles    LINER2
ASSIGNMA    Stainles    LINER3
ASSIGNMA    Stainles    LINER4
ASSIGNMA    Stainles    LINER5
ASSIGNMA         AIR   CAVITY1
ASSIGNMA         AIR   CAVITY2
ASSIGNMA    Stainles     DOOR1
ASSIGNMA        LEAD     DOOR2
ASSIGNMA    ALUMINUM   HOLDER1
ASSIGNMA         AIR   HOLDER2
ASSIGNMA    Polymeth   HOLDER3
ASSIGNMA         AIR   HOLDER4
ASSIGNMA    ALUMINUM      DET1
ASSIGNMA         AIR      DET2
ASSIGNMA    ALUMINUM      DET3
ASSIGNMA    ALUMINUM      DET4
ASSIGNMA         AIR      DET5
ASSIGNMA       Mylar      DET6
ASSIGNMA       BORON   BOROUT1
```

```
ASSIGNMA       BORON   BOROUT2
ASSIGNMA       BORON   BOROUT3
ASSIGNMA       BORON   BOROUT4
ASSIGNMA    GERMANIU       GE1
ASSIGNMA    GERMANIU       GE2
ASSIGNMA    GERMANIU       GE3
ASSIGNMA    GERMANIU       GE4
ASSIGNMA       BORON   BOROUT5
ASSIGNMA    GERMANIU       GE5
ASSIGNMA     LITHIUM     LITH1
ASSIGNMA     LITHIUM     LITH2
ASSIGNMA     LITHIUM     LITH3
ASSIGNMA     LITHIUM     LITH4
ASSIGNMA     LITHIUM     LITH5
ASSIGNMA         AIR     HOLE1
ASSIGNMA         AIR     HOLE2
ASSIGNMA         AIR     HOLE3
ASSIGNMA         AIR     HOLE4
ASSIGNMA         AIR     HOLE5
EMF
*EMFCUT           0.0       0.0                       LITHIUM
1.0PROD-CUT
EMFFLUO           1.  GERMANIU
EMFRAY            1.       GE1       GE5
IONTRANS    OPTIPHOT
*USRBIN          10.    ENERGY      -21.       20.      42.0       20.
*USRBIN         -20.       0.0      -20.      100.      100.
100.&
DETECT           0.0      1E-9  1.024E-3                 1.       GE1
DETECT           0.0       GE2       GE3       GE4       GE5          &
* Set the random number seed
RANDOMIZ          1.
* Set the number of primary histories to be simulated in the run
START       1181500.
STOP
```